
Robust Distributed Learning under Resource Constraints: Decentralized Quantile Estimation via (Asynchronous) ADMM

Anna van Elst¹ Igor Colin¹ Stephan Cléménçon¹

Abstract

Specifications for decentralized learning on resource-constrained edge devices require algorithms that are communication-efficient, robust to data corruption, and lightweight in memory usage. While state-of-the-art gossip-based methods satisfy the first requirement, achieving robustness remains challenging. Asynchronous decentralized ADMM-based methods have been explored for estimating the median, a statistical centrality measure that is notoriously more robust than the mean. However, existing approaches require memory that scales with node degree, making them impractical when memory is limited. In this paper, we propose AsylADMM, a novel gossip algorithm for decentralized median and quantile estimation, primarily designed for asynchronous updates and requiring only two variables per node. We analyze a synchronous variant of AsylADMM to establish theoretical guarantees and empirically demonstrate fast convergence for the asynchronous algorithm. We then show that our algorithm enables quantile-based trimming, geometric median estimation, and depth-based trimming, with quantile-based trimming empirically outperforming existing rank-based methods. Finally, we provide a novel theoretical analysis of rank-based trimming via Markov chain theory.

1. Introduction

Decentralized learning has become essential for large-scale machine learning, driven by the rapid development of edge AI systems. In many applications, data is generated and processed directly on resource-constrained devices such as connected sensors or mobile phones, which cannot rely on centralized architectures due to communication, energy, or privacy constraints. Gossip learning methods are partic-

ularly appealing in this context: they rely on lightweight peer-to-peer communication, avoid global coordination, and scale naturally with network size (Boyd et al., 2006; 2011). Despite these advantages, most gossip learning algorithms lack robustness to corrupted data—even a small fraction of faulty measurements can significantly degrade performance (Van Elst et al., 2025b; Ayadi et al., 2017). While outlier trimming methods are standard in centralized settings, they are challenging to deploy in distributed networks where nodes only have access to local information.

The use of robust statistics such as the median or trimmed/winsorized means, which are less sensitive to extreme values (Huber & Ronchetti, 2011), may indeed address the issue. To compute trimmed means in this context, decentralized algorithms based on statistical inference have been recently proposed (Van Elst et al., 2025b), while, for medians and more generally empirical quantiles, optimization-based approaches (M -estimation) are more natural, as such statistics minimize a pinball loss. Because such losses are non-smooth, proximal methods are preferred over slow-converging subgradient methods (Iutzeler, 2017). ADMM (Boyd et al., 2011) offers two key advantages: as a proximal method, it effectively handles non-smoothness and, as a splitting method, it circumvents the non-linearity of the proximal operator by decoupling consensus constraints from local optimization. However, existing decentralized ADMM algorithms are either synchronous (Wei & Ozdaglar, 2012) or, when asynchronous, require additional variables and incur significant memory overhead (Iutzeler, 2017; Bianchi et al., 2015). Our main contributions, which address these limitations, are as follows:

- We propose **AsylADMM**, a novel **Asynchronous** and **Lite** ADMM-based gossip algorithm for median and quantile decentralized estimation. Compared to existing asynchronous ADMM methods, our algorithm offers several advantages:
 - (a) *Memory-efficiency*: each node stores only two variables, compared to $2d + 1$ variables required in previous work, denoting by d the node degree.
 - (b) *Fast Convergence*: through extensive experiments across a wide range of networks and data distributions, we provide empirical evidence demonstrating that AsylADMM con-

¹LTCI, Télécom Paris, Institut Polytechnique de Paris, France. Correspondence to: Anna van Elst <anna.vanelst@telecom-paris.fr>.

verges faster than its competitors.

- We apply AsylADMM to quantile-based trimming and geometric median estimation, as well as depth-based trimming. Additionally, we empirically show that quantile-based trimming outperforms rank-based trimming methods for standard graph topologies and contaminated distributions.
- We provide two novel theoretical results: (a) a new convergence analysis for the synchronous version of AsylADMM, which we believe provides a preliminary basis for understanding the asynchronous case; (b) a new theoretical analysis of rank-based trimming via Markov chain theory, complementing the approach in [Van Elst et al. \(2025b\)](#).

2. Background and Preliminaries

This section reviews the decentralized optimization and quantile estimation methods documented in the literature, against which our approaches compare favorably.

2.1. Decentralized Optimization

We begin by reviewing the main methods of decentralized optimization for non-smooth convex objectives. Here and throughout, we denote scalars by lowercase letters $x \in \mathbb{R}$, vectors by boldface lowercase letters $\mathbf{x} \in \mathbb{R}^n$, and matrices by boldface uppercase letters $\mathbf{X} \in \mathbb{R}^{m \times n}$. We set $[n] := \{1, \dots, n\}$ and write $\{\mathbf{e}_k : k \in [n]\}$ for \mathbb{R}_n 's canonical basis, $\mathbb{I}\{\mathcal{A}\} \in \{0, 1\}$ for the indicator function of any event \mathcal{A} , \mathbf{M}^\top for the transpose of any matrix \mathbf{M} , $|F|$ the cardinality of any finite set F , \mathbf{I}_n for the identity matrix in $\mathbb{R}^{n \times n}$, $\mathbf{1}_n$ for the vector in \mathbb{R}^n whose coordinates are all equal to 1, $\|\cdot\|$ for the usual ℓ_2 -norm, and $\lfloor \cdot \rfloor$ for the floor function. The set of edges defining the network is denoted by $E \subset [n]^2$.

Problem Formulation. Consider a distributed optimization problem over a connected network of $n \geq 1$ agents, where each agent $i \in \{1, \dots, n\}$ has a closed, proper, convex, and non-smooth local objective f_i . The goal is to solve the minimization problem below collaboratively:

$$\operatorname{argmin}_{\mathbf{x} \in \mathbb{R}^d} \sum_{i=1}^n f_i(\mathbf{x}). \quad (1)$$

Gossip-based methods address this problem by alternating local updates with neighbor averaging ([Nedic & Ozdaglar, 2009; Duchi et al., 2011](#)).

Subgradient Descent. Each node performs local (sub)gradient updates and averages its estimate through pairwise communication. Introduced in [Nedic & Ozdaglar \(2009\)](#), the method converges at rate $\mathcal{O}(1/\sqrt{t})$, where $t \geq 1$ denotes the number of iterations. However, it is sensitive to step-size selection, especially for non-smooth objectives, and often converges slowly in practice.

Proximal Methods. Proximal methods are well-suited for non-smooth objectives. A canonical example is the proximal point algorithm (PPA) with step size $\rho > 0$,

$$\mathbf{x}^{t+1} = \operatorname{prox}_{\rho f}(\mathbf{x}^t) := \operatorname{argmin}_{\mathbf{x}} \left\{ f(\mathbf{x}) + \frac{1}{2\rho} \|\mathbf{x} - \mathbf{x}^t\|^2 \right\},$$

which can be interpreted as an implicit gradient descent. Distributed variants such as P-EXTRA have been proposed ([Shi et al., 2015](#)), but they do not naturally extend to fully decentralized gossip-based settings due to the non-linearity of the proximal operator. In contrast, decentralized ADMM methods are widely used for minimizing sums of convex non-smooth functions in a decentralized setting, as they decouple local optimization from consensus constraints and hence support gossip-based asynchronous implementations ([Shi et al., 2014; Yang et al., 2022; Boyd et al., 2011](#)).

Synchronous ADMM. We focus on edge-based (gossip) methods, as studied in ([Iutzeler et al., 2013](#)). For clarity of notation, we consider the scalar case in the remainder of the paper, as motivated by quantile estimation; most of the results extend to the general setting. Problem (1) can be reformulated as $\operatorname{argmin}_{\mathbf{x} \in \mathbb{R}^n} \sum_{i=1}^n f_i(x_i)$ subject to $x_i = x_j$ for all $(i, j) \in E$. These constraints ensure that the nodes' estimates reach consensus (assuming the graph is connected), while keeping the problem decentralized. This can be written in ADMM form as in ([Iutzeler et al., 2013](#)):

$$\begin{aligned} \min_{\mathbf{x} \in \mathbb{R}^n, \mathbf{z} \in \mathbb{R}^{2m}} \quad & f(\mathbf{x}) + g(\mathbf{z}) \\ \text{subject to} \quad & \mathbf{Mx} = \mathbf{z} \end{aligned}, \quad (2)$$

where by $m = |E|$ is the number of edges and $f(\mathbf{x}) \triangleq \sum_{i=1}^n f_i(x_i)$. The matrix $\mathbf{M} \in \mathbb{R}^{2|E| \times n}$ is constructed as $\mathbf{M} = [\mathbf{M}_e]_{e \in E}$, where for each edge $e = (i, j)$, the submatrix $\mathbf{M}_e \in \mathbb{R}^{2 \times n}$ extracts the corresponding node variables: $\mathbf{M}_e \mathbf{x} = [x_i, x_j]^\top = \mathbf{z}_e$. Denoting by $\iota_C : \mathbb{R}^{2m} \rightarrow \{0, +\infty\}$ the convex indicator function of $C = \operatorname{span}(\mathbf{1}_2)$, $g(\mathbf{z}) \triangleq \sum_{e \in E} \iota_C(\mathbf{z}_e)$. The indicator functions $\iota_C(\mathbf{z}_e)$ enforce the hard constraints $x_i = x_j$ for each edge $e = (i, j)$, ensuring consensus on a connected network. Note that, by construction, the matrix \mathbf{M} is full column-rank, so Problem (2) is well-posed. Finally, we recall that the proximal operator of ι_C coincides with the orthogonal projection Π_C onto C . A synchronous decentralized ADMM for the above problem has been proposed and analyzed theoretically ([Shi et al., 2014; Iutzeler et al., 2013; 2015](#)). [Iutzeler et al. \(2015\)](#) prove that \mathbf{x}^* is a minimizer of Problem (1) if and only if (x^*, \dots, x^*) is a minimizer of Problem (2).

Asynchronous ADMM. Asynchronous methods are often more practical than synchronous ones, as they avoid global coordination, tolerate communication delays, and scale well with large networks. An asynchronous decentralized ADMM was proposed in [Iutzeler et al. \(2013\)](#). Its main limitation is that each node k must store $2d_k$ auxiliary

variables associated with its incident edges: this memory requirement becomes significant when the graph is dense or when nodes have limited memory capacity. Another asynchronous ADMM method has been proposed in (Wei & Ozdaglar, 2013). However, when applied to our problem, its edge-based reformulation does not converge, see the illustrative experimental results in Appendix J. In addition, an asynchronous decentralized primal-dual algorithm, referred to as DAPD, has been proposed in (Bianchi et al., 2015). Like the previous methods, DAPD incurs significant memory overhead at each node, as it requires the additional variables $\bar{x} \in \mathbb{R}^{2|E|}$ and $\lambda \in \mathbb{R}^{2|E|}$. These algorithms are reviewed in more detail in Appendix A.

Convergence Analysis of Decentralized ADMM. In the synchronous setting, the convergence analysis of ADMM reduces to standard results established for centralized ADMM (Boyd et al., 2011). In the asynchronous setting, several methods have been applied to derive convergence guarantees: using random Gauss-Seidel iterations applied to the Douglas-Rachford operator (Iutzeler et al., 2013), or by framing the updates as stochastic coordinate descent on an averaged operator (Bianchi et al., 2015). However, these techniques do not directly apply to the approach we promote here. Convergence is proved in Wei & Ozdaglar (2013) using martingale limit theory. However, as pointed out therein, the edge-based formulation does not satisfy one of the principal assumptions required for the convergence proof. This seems consistent with the empirical results presented in Appendix J, which clearly show a lack of convergence.

2.2. (Decentralized) Quantile Estimation

Here, we review the main methods for quantile and median estimation (Wasserman, 2013).

M-estimation. The α -quantiles of a set of observed data points a_1, a_2, \dots, a_n can be recovered as minimizers of the following optimization problem:

$$\operatorname{argmin}_{x \in \mathbb{R}} f_n(x) \triangleq \sum_{i=1}^n L_\alpha(a_i - x) , \quad (3)$$

where $L_\alpha(z) := (\alpha - \mathbb{I}\{z \leq 0\})z$ is the *pinball loss*. We note that the problem is equivalent to that presented in Iutzeler (2017) after dividing the pinball loss by $1 - \alpha$. Hence, we adopt the notation and results from that work, defining $f_a^\beta : x \mapsto L_\alpha(a - x)/(1 - \alpha)$ with $\beta = \alpha/(1 - \alpha)$. For $a \in \mathbb{R}$ and $\beta > 0$, f_a^β is convex and continuous. Although it is non-differentiable, its proximal operator has a

known closed-form solution given by Iutzeler (2017):

$$\begin{aligned} \operatorname{prox}_{\gamma f_a^\beta}(z) &\triangleq \operatorname{argmin}_{w \in \mathbb{R}} \left\{ f_a^\beta(w) + \frac{1}{2\gamma} \|w - z\|^2 \right\} \\ &= \begin{cases} z + \gamma\beta, & \text{if } z < a - \gamma\beta \\ z - \gamma, & \text{if } z > a + \gamma \\ a, & \text{if } z \in [a - \gamma\beta, a + \gamma] , \end{cases} \end{aligned}$$

which naturally leads us to employ proximal methods.

Rank-based methods. Quantiles can be viewed as specific L -statistics, i.e. linear combinations of order statistics: the α -quantile corresponds to the α -th order statistic (or an interpolation thereof). As order statistics are determined simply by ranking the observations, which can be done quickly in the centralized framework, estimating the α -quantile reduces to identifying the observation with rank $\lfloor \alpha n \rfloor$. Asynchronous gossip methods have been developed for distributed ranking, enabling each node to estimate the rank of its local observation within the network, and have been extended to estimate L -statistics (Van Elst et al., 2025a;b). However, as they require estimating the ranks of all observations rather than directly computing the target quantile, such methods are slow when applied in a decentralized setting, in comparison to approaches based on decentralized M -estimation.

3. AsyIADMM: Asynchronous Algorithm for Decentralized Quantile Estimation

This section presents the problem formulation and framework, describes the proposed asynchronous algorithm along with its empirical evaluation, and derives the convergence analysis of the synchronous variant.

3.1. Problem Formulation and Framework

We consider a decentralized setting with $n \geq 2$ observations a_1, \dots, a_n , each held by a distinct node in a communication network. The network topology is modeled by an undirected, connected, non-bipartite graph $G = ([n], E)$, where node $k \in [n]$ holds observation a_k . Communication follows the randomized gossip protocol introduced by (Boyd et al., 2006): at each time step, an edge $e \in E$ is selected with probability $p_e > 0$, and the two incident nodes exchange information. We use asynchronous updates with standard edge sampling: $p_e = (1/n) \cdot (1/d_i + 1/d_j)$ for $e = (i, j) \in E$, where d_i, d_j are the node degrees. Our objective is to estimate medians and quantiles in this decentralized setting using the optimization-based approach via pinball loss minimization described in Section 2.2. Since pinball losses are proper and convex but non-smooth, proximal methods are naturally suited to this problem. We adopt the asynchronous ADMM framework of Iutzeler et al. (2013) and use the formulation given in Problem (2).

3.2. The AsylADMM Algorithm

A major limitation of both Async-ADMM and DAPD is their considerable memory overhead, as discussed in Section 2.1. In this section, we propose an asynchronous ADMM algorithm that addresses this issue by: (i) using a single aggregate for the dual variables, and (ii) eliminating storage of neighbor values. These modifications simplify primal and dual updates while reducing auxiliary variables per node. We derive our algorithm by returning to Problem (2), formulated via the *simplified* augmented Lagrangian:

$$\mathcal{L}_\rho(\mathbf{x}, \mathbf{z}, \mathbf{y}) = f(\mathbf{x}) + \mathbf{y}^\top (\mathbf{z} - \mathbf{M}\mathbf{x}) + \frac{\rho}{2} \|\mathbf{z} - \mathbf{M}\mathbf{x}\|^2,$$

where $g(\mathbf{z}) = 0$, since the consensus step, as detailed hereafter, ensures that $\mathbf{z}_e = (z_e, z_e) \in C$ for all $e \in E$. We note, however, that the theoretical derivation still relies on the function g . Denote by d_k the degree of node k , by N_k the set of edges incident to node k , and by $\mathcal{N}(k)$ the set of its neighbors. The Lagrangian admits a decomposition across nodes. Considering the local Lagrangian for node k

$$\mathcal{L}_\rho^{(k)}(\mathbf{x}_k, \mathbf{z}_k, \mathbf{y}_k) = f_k(\mathbf{x}_k) + \sum_{e \in N_k} y_{e,k} (z_e - x_k) + \frac{\rho}{2} (z_e - x_k)^2,$$

where $\mathbf{z}_k = (z_e)_{e \in N_k}$ and $\mathbf{y}_k = (y_{e,k})_{e \in N_k}$, we have by construction: $\mathcal{L}_\rho(\mathbf{x}, \mathbf{z}, \mathbf{y}) = \sum_{k=1}^n \mathcal{L}_\rho^{(k)}(\mathbf{x}_k, \mathbf{z}_k, \mathbf{y}_k)$.

To develop our asynchronous algorithm AsylADMM, we begin with its synchronous counterpart. In the synchronous setting, all nodes perform their updates simultaneously and exchange information with their neighbors at each iteration. The algorithm initializes the primal variables as $x_k = a_k$ for all k , where a_k denotes the observation at node k , and the dual variables as $y_{e,k} = 0$ for all $e \in N_k$. Given the current iterates $(\mathbf{x}, \mathbf{z}, \mathbf{y})$, the algorithm proceeds as follows:

- **Consensus step:** Compute $\mathbf{z}^+ = [z_e^+ \mathbf{1}_2]_{e \in E}$ where for $e = (i, j)$, $z_e^+ = (x_i + x_j)/2$.
- **Dual update:** For all nodes $k \in [n]$ and $e \in N_k$, set $y_{e,k}^+ = y_{e,k} + \rho(z_e^+ - x_k)$.
- **Primal update:** For all nodes $k \in [n]$, set $x_k^+ \in \operatorname{argmin}_{x_k} \mathcal{L}_\rho^{(k)}(\mathbf{x}_k, \mathbf{z}_k^+, \mathbf{y}_k^+)$ where $\mathbf{z}_k^+ = (z_e^+)_{e \in N_k}$ and $\mathbf{y}_k^+ = (y_{e,k}^+)_{e \in N_k}$.

Note that this formulation employs a reordered variant of ADMM: rather than the standard x - z - y update sequence (Boyd et al., 2011), we adopt a z - y - x ordering similar to Bianchi et al. (2015). This reordering offers two advantages. First, it eliminates the need to store additional variables, as the x -update depends only on quantities from the current iteration. Second, it yields a particularly simple update structure consisting of (i) a consensus step between connected nodes, followed by (ii) local updates at each node.

To reduce the number of auxiliary variables that must be stored, we introduce the reparameterization $\hat{z}_k = \sum_{e \in N_k} z_e/d_k$ and $\hat{\mu}_k = \sum_{e \in N_k} y_{e,k}/d_k$. With this choice, the consensus step simplifies to $\hat{z}_k^+ = (\hat{x}_k + x_k)/2$, where \hat{x}_k denotes the average of the neighboring iterates. Moreover, the dual update depends only on \hat{z}_k and x_k , and the primal update reduces to a simple proximal step. This is formalized in the following lemma.

Lemma 3.1. *The following statements are equivalent:*

- $x_k \in \operatorname{argmin}_x \mathcal{L}_\rho^{(k)}(x, \mathbf{z}_k, \mathbf{y}_k)$;
- $x_k = \operatorname{prox}_{f_k/(\rho d_k)}(\hat{z}_k + \hat{\mu}_k/\rho)$, where $\hat{z}_k = \mathbf{1}_{d_k}^\top \mathbf{z}_k/d_k$ and $\hat{\mu}_k = \mathbf{1}_{d_k}^\top \mathbf{y}_k/d_k$.

Proof. Expanding the terms in $\mathcal{L}_\rho^{(k)}(x_k, \mathbf{z}_k, \mathbf{y}_k)$ and dropping those independent of x_k , we apply the reparameterization and complete the square to obtain the proximal form. The detailed derivation is provided in Appendix B. \square

This reformulation replaces the edge-based variables with node-based quantities, reducing storage requirements. Using the reparameterization and Lemma 3.1, the algorithm can be reformulated as outlined in Algorithm 1.

Algorithm 1 Synchronous Variant

```

1: Input: Initial vectors  $a_1, \dots, a_n$ ; step size  $\rho > 0$ .
2: Initialization:  $\forall k, x_k \leftarrow a_k, \hat{\mu}_k \leftarrow 0$ .
3: for  $t = 0, 1, \dots$  do
4:   for all  $k = 1, \dots, n$  in parallel do
5:     Compute average:  $\hat{x}_k \leftarrow \sum_{l \in \mathcal{N}(k)} x_l/d_k$ .
6:     Set  $\hat{z}_k \leftarrow (\hat{x}_k + x_k)/2$ .
7:     Set  $\hat{\mu}_k \leftarrow \hat{\mu}_k + \rho(\hat{z}_k - x_k)$ .
8:     Set  $x_k \leftarrow \operatorname{prox}_{f_k/(\rho d_k)}(\hat{z}_k + \hat{\mu}_k/\rho)$ .
9:   end for
10: end for

```

We now derive our asynchronous algorithm using the following heuristics. As in the synchronous case, we rely on Lemma 3.1 by using an aggregate of the dual variables in the proximal update. However, we keep z_e as is, without aggregation. This choice is motivated by the fact that $\hat{\mu}_k$ admits a clean update in terms of the constraint associated with edge e , whereas \hat{z}_k does not. Moreover, we observed that using z_e instead of \hat{z}_k in the update does not significantly affect convergence in practice. The resulting algorithm is called **AsylADMM** and is outlined in Algorithm 2.

A notable advantage is the simplicity of the update rules, which require only one communication step and reduce storage. Empirically, we observed that using only $y_{e,k}$ instead of the aggregate $\hat{\mu}_k$ leads to divergence. This can be explained by the fact that $\hat{\mu}_k$ encodes information about consensus constraints with all neighboring nodes, not just the currently active edge.

Algorithm 2 AsylADMM: Async & Lite ADMM

```

1: Input: Initial vectors  $a_1, \dots, a_n$ ; step size  $\rho > 0$ .
2: Initialization: For all nodes  $k = 1, \dots, n$ :
3:    $x_k \leftarrow a_k$ ,  $\hat{\mu}_k \leftarrow 0$ .
4: for  $t = 0, 1, \dots$  do
5:   Draw  $e = (i, j) \in E$  with probability  $p_e$ .
6:   Compute average:  $z_e \leftarrow \frac{1}{2}(x_i + x_j)$ .
7:   Agents  $k \in \{i, j\}$  update:
       $\hat{\mu}_k \leftarrow \hat{\mu}_k + \rho(z_e - x_k)/d_k$  ;
       $x_k \leftarrow \text{prox}_{\frac{f_k}{\rho d_k}}(z_e + \hat{\mu}_k/\rho)$ .
8: end for

```

3.3. Empirical Comparison with Existing Methods

Here, we present a series of experiments comparing our novel asynchronous ADMM algorithm (AsylADMM) with several existing distributed optimization methods: DAPD from [Bianchi et al. \(2015\)](#), AsyncADMM from [Iutzeler et al. \(2013\)](#), and distributed subgradient descent from [Nedic & Ozdaglar \(2009\)](#). We evaluate performance across multiple problem settings, including median and quantile estimation, as well as various network topologies. The code for our experiments is available in the supplementary material.

Setup. We evaluate distributed optimization methods on quantile estimation problems using contaminated data. Unless otherwise specified, experiments use a network of $n = 101$ nodes arranged in a geometric graph with 507 edges. Each node observes data from a contaminated Gaussian distribution: 80% from $\mathcal{N}(10, 3^2)$ and 20% from $\mathcal{N}(30, 5^2)$. We use an odd sample size to ensure a unique median. All results report mean absolute error over 100 independent trials. For each trial, the step size ρ is drawn uniformly from $[0.1, 1.0]$ and applied consistently across all algorithms, and data assignments are randomly shuffled across nodes. This design evaluates robustness to both hyperparameter selection and data distribution on the graph.

Plot (a). We compare four methods: AsylADMM, DAPD, AsyncADMM, and subgradient descent. Note that the subgradient method is not fully asynchronous (see Appendix A). AsylADMM converges significantly faster, followed by DAPD and AsyncADMM. Subgradient descent shows fast initial progress but struggles in later iterations and exhibits high sensitivity to step size. DAPD and AsyncADMM show noticeably higher variance across runs, while AsylADMM proves more stable and easier to tune. The performance gap among the ADMM variants comes from how each estimates the neighborhood average \hat{z}_k . AsyncADMM uses outdated values: $\hat{z}_k = \sum_{e \in N_k} z_e^{\text{old}}/d_k$ with $z_e^{\text{old}} = (x_k^{\text{old}} + x_l^{\text{old}})/2$. DAPD combines current local and outdated neighbor information: $\hat{z}_k = (x_k^{\text{new}} + \bar{x}_k^{\text{old}})/2$. AsylADMM uses current information from both endpoints: $\hat{z}_k = (x_k^{\text{new}} + x_l^{\text{new}})/2$. This heuristic performs remarkably well in practice, thanks

to its use of up-to-date information and the underlying gossip principle, in which repeated pairwise averaging naturally converges toward an accurate global average.

Plot (b). We conduct a similar experiment targeting the $\alpha = 0.3$ quantile under the same contaminated Gaussian distribution, network topology and settings. All algorithms converge more slowly when estimating the quantile, suggesting this problem is slightly harder, potentially as a result of the contaminated distribution. Here, DAPD and AsyncADMM show even higher variability, again highlighting the difficulty of the problem. AsylADMM, however, remains consistently stable and competitive.

Plot (c). We evaluate AsylADMM on median estimation on three graph structures with varying connectivity $c = \lambda_2/|E|$, where λ_2 denotes the second smallest eigenvalue of the graph Laplacian. The topologies are: Watts-Strogatz ($|E| = 202$, $c = 2.28 \times 10^{-3}$), geometric ($|E| = 507$, $c = 4.34 \times 10^{-4}$), and cycle ($|E| = 101$, $c = 3.83 \times 10^{-5}$). Results demonstrate that graph connectivity directly influences convergence rate.

Additional experiments. Appendix C presents additional empirical results following the setup of Figure 1 and investigating the impact of several settings. The key findings are as follows. (a) AsyncADMM and DAPD converge significantly slower on dense graphs, while AsylADMM performs consistently well even on large networks ($n > 1000$), confirming scalability. (b) All algorithms degrade at extreme quantiles ($\alpha \in \{0.1, 0.9\}$) due to tail contamination, but AsylADMM shows less sensitivity than baselines, further demonstrating its robustness. (c) AsylADMM converges reliably, though more slowly, when increasing data contamination (40%) or using Cauchy-distributed data.

3.4. Convergence Analysis of Synchronous Variant

In this section, we present a novel convergence analysis for the synchronous setting, which may serve as a foundation for the theoretical analysis of the asynchronous case. Throughout, we assume that the unaugmented Lagrangian admits a saddle point. Under this assumption, [Boyd et al. \(2011\)](#) established two convergence results for standard ADMM: residual convergence, whereby the iterates approach feasibility ($\mathbf{z}^t - \mathbf{Mx}^t \rightarrow 0$ as $t \rightarrow \infty$), and objective convergence, whereby the objective value approaches the optimal values ($f(\mathbf{x}^t) + g(\mathbf{z}^t) \rightarrow p^*$ as $t \rightarrow \infty$). We establish analogous results for our reordered variant using a modified Lyapunov function. To this end, we first establish two inequalities that bound $f(\mathbf{x}) - f(\mathbf{x}^*)$ and $f(\mathbf{x}^*) - f(\mathbf{x})$, respectively. The complete derivation and detailed steps are provided in Appendix B.

Let $(\mathbf{x}^*, \mathbf{z}^*, \mathbf{y}^*)$ be a saddle point of \mathcal{L}_0 . Define the primal residual $\mathbf{r}^{t+1} := \mathbf{z}^{t+1} - \mathbf{Mx}^{t+1}$ and the errors $\tilde{\mathbf{x}}^{t+1} =$

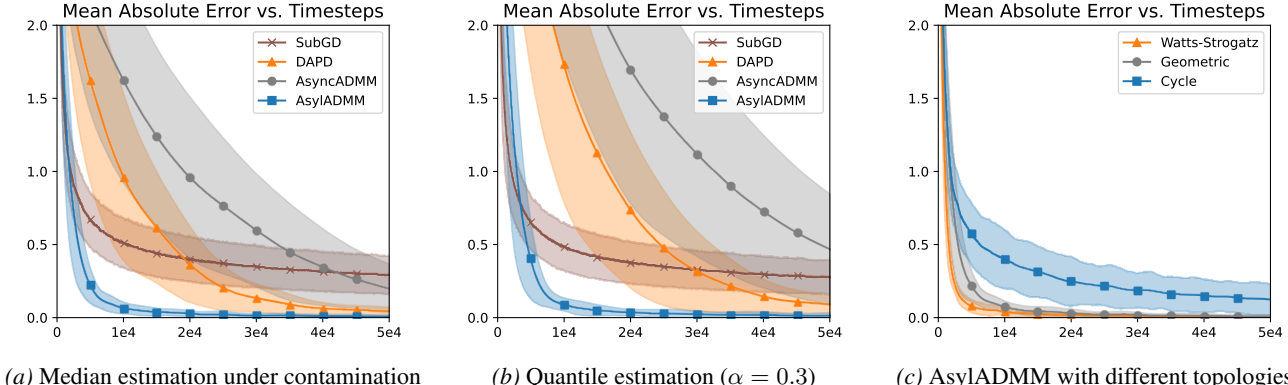


Figure 1. Convergence performance of AsylADMM on contaminated Gaussian data. Plots (a) and (b) compare AsylADMM with existing optimization methods for median and quantile ($\alpha = 0.3$) estimation. Plot (c) shows the impact graph topology on AsylADMM convergence, comparing Watts-Strogatz, geometric, and cycle graphs with varying connectivity levels. All plots show mean absolute error versus number of iterations, averaged over 100 trials with corresponding standard deviation.

$\mathbf{x}^{t+1} - \mathbf{x}^*$ and $\tilde{\mathbf{y}}^{t+1} = \mathbf{y}^{t+1} - \mathbf{y}^*$. The first inequality is

$$f(\mathbf{x}^{t+1}) - f(\mathbf{x}^*) \leq (\rho \mathbf{M} \tilde{\mathbf{x}}^{t+1} - \mathbf{y}^{t+1})^\top \mathbf{r}^{t+1}, \quad (\text{I})$$

while the second inequality is

$$f(\mathbf{x}^*) - f(\mathbf{x}^{t+1}) \leq \mathbf{y}^*^\top \mathbf{r}^{t+1}. \quad (\text{II})$$

The following lemma establishes that a suitably chosen function decreases at each iteration.

Lemma 3.2. Define $V^t = \|\tilde{\mathbf{y}}^t - \rho \mathbf{M} \tilde{\mathbf{x}}^t\|^2$. Then,

$$\forall t \geq 0, \quad V^{t+1} - V^t \leq -\rho^2 \|\mathbf{r}^{t+1}\|^2.$$

Proof. Define $\tilde{\mathbf{q}}^t := \tilde{\mathbf{y}}^t - \rho \mathbf{M} \tilde{\mathbf{x}}^t$. Applying the identity $\|\mathbf{a}\|^2 - \|\mathbf{b}\|^2 = 2\mathbf{a}^\top(\mathbf{a} - \mathbf{b}) - \|\mathbf{a} - \mathbf{b}\|^2$ with $\mathbf{a} = \tilde{\mathbf{q}}^{t+1}$, $\mathbf{b} = \tilde{\mathbf{q}}^t$, and $\mathbf{a} - \mathbf{b} = \rho \mathbf{r}^{t+1}$, we obtain

$$V^{t+1} - V^t = 2\rho(\tilde{\mathbf{y}}^{t+1} - \rho \mathbf{M} \tilde{\mathbf{x}}^{t+1})^\top \mathbf{r}^{t+1} - \|\rho \mathbf{r}^{t+1}\|^2.$$

Summing inequalities (I) and (II) yields $(\tilde{\mathbf{y}}^{t+1} - \rho \mathbf{M} \tilde{\mathbf{x}}^{t+1})^\top \mathbf{r}^{t+1} \leq 0$, and substituting into the expression above completes the proof. \square

We can now establish the convergence of Algorithm 1.

Theorem 3.3. Let $\{(\mathbf{x}^t, \mathbf{z}^t, \mathbf{y}^t)\}_{t>0}$ be the sequence generated by Algorithm 1. Then, for $t > 0$:

$$\lim_{t \rightarrow \infty} \|\mathbf{r}^t\| = 0, \quad \lim_{t \rightarrow \infty} f(\mathbf{x}^t) = f(\mathbf{x}^*).$$

Proof. By Lemma 3.2, the Lyapunov function V^t decreases at each iteration by an amount proportional to the squared residual norm. Since V^t is non-negative and bounded for all t , the sequence $\{\tilde{\mathbf{y}}^t - \rho \mathbf{M} \tilde{\mathbf{x}}^t\}$ remains bounded. Summing the inequality from Lemma 3.2 over all iterations yields

$$\rho^2 \sum_{t=0}^{\infty} \|\mathbf{r}^{t+1}\|^2 \leq V^0 < +\infty.$$

Convergence of this series implies that $\|\mathbf{r}^t\| \rightarrow 0$ as $t \rightarrow \infty$, establishing the first claim. We combine the boundedness of $\{\tilde{\mathbf{y}}^t - \rho \mathbf{M} \tilde{\mathbf{x}}^t\}$ with the residual convergence just established. Applying inequality (I), we obtain $|f(\mathbf{x}^t) - f(\mathbf{x}^*)| \rightarrow 0$, which completes the proof. \square

4. Applications: Geometric Median and Quantile/Depth-Based Trimming

This section details the application of Algorithm 2 to three problems: geometric median estimation, quantile-based trimming, and depth-based trimming. We begin by describing each problem and the proposed methods. We then present a novel theoretical analysis of rank-based trimming, followed by empirical validation of our methods.

4.1. Background and Methods

Geometric median. A natural multivariate extension of the univariate median is the geometric median, also known as the spatial median. Like the coordinate-wise median, it achieves the highest possible breakdown point of 1/2 (Lopuhaä & Rousseeuw, 1991). However, the geometric median offers several advantages over its coordinate-wise counterpart: it has superior asymptotic efficiency and guarantees that the estimate lies within the convex hull of the data-points (Oja, 2013; Minsker, 2015; Serfling, 2006). Similar to the median, its proximal operator has a closed-form solution (Parikh et al., 2014), which can be directly used in Algorithm 2; see Appendix D for further details.

Quantile/rank-based trimming. Quantiles play a key role in the construction of trimming rules for robust statistical methods. Trimming excludes observations falling in the tails of the empirical distribution, typically those below the α -th quantile q_α or above the $(1 - \alpha)$ -th quantile $q_{1-\alpha}$. The

resulting trimmed sample forms the basis for estimators, such as the trimmed mean, that are more robust to data contamination. Note that while the median is also a robust estimator, the trimmed mean can, in certain cases, provide a more efficient estimate of location than the sample median (Oosterhoff, 1994). Similarly, in robust optimization, one can trim (*i.e.*, discard) large gradients that would otherwise disrupt the optimization process. We consider two trimming rules. In quantile-based trimming, an observation or gradient is included if it lies within $[q_\alpha, q_{1-\alpha}]$, requiring two instances of AsyLADMM for estimating each quantile. In rank-based trimming, each node maintains a local rank estimate and includes its observation or gradient if the corresponding rank falls within $[m+1, n-m]$, where n denotes the sample size and $m = \lfloor \alpha n \rfloor$ (Van Elst et al., 2025b). For this rank-based rule, we use Asynchronous GoRank (Van Elst et al., 2025a). For trimmed mean estimation, we use Adaptive GoTrim (Van Elst et al., 2025a) with the two rules described above. The aforementioned algorithms are outlined in Appendix D, along with an analysis showing how trimming weight errors are controlled by quantile estimation and ranking errors. The robust optimization case, with a robust regression example, is detailed in Appendix I.

Depth-based Trimming. In \mathbb{R}^d for $d \geq 2$, unlike the univariate case, there is no natural ordering of vectors. Data depth functions address this by assigning each point a value reflecting how central it lies relative to a data cloud, thereby generalizing the concept of rank to the multivariate setting (Mosler, 2013; Serfling, 2006). This enables the construction of α -trimmed multivariate estimators, which discard the fraction α of points with the lowest depth. Among the many definitions of data depth, L_2 -depth (Mosler, 2013) is particularly convenient for our decentralized setting. Indeed, recall the definition of the L_2 -depth of \mathbf{z} :

$$D^{L_2}(\mathbf{z} \mid \mathbf{x}_1, \dots, \mathbf{x}_n) = \left(1 + \frac{1}{n} \sum_{i=1}^n \|\mathbf{z} - \mathbf{x}_i\| \right)^{-1}.$$

A key observation is that the mean $(1/n) \sum_{i=1}^n \|\mathbf{z} - \mathbf{x}_i\|$ can be estimated using a running average at each node. The resulting procedure is outlined in Appendix D (see GoDepth); it builds on ideas similar to those of GoRank. However, since depth values are only meaningful in relation to one another, we must also rank them across nodes or find the α -quantile of the estimated depths. Once each node has estimated its L_2 depth, we can apply AsyLADMM to estimate the α -quantile of these depths, which then serves as the trimming threshold for computing the α -trimmed multivariate mean. In fact, since AsyLADMM is an optimization algorithm, we can do this simultaneously by updating the input data of AsyLADMM with the latest depth estimation at each step (see Appendix D for further details).

4.2. Theoretical Analysis of Rank-Based Trimming

Here, we provide novel theoretical analysis of rank-based trimming introduced in Van Elst et al. (2025b). We use the framework introduced in section 3. The rank of a_k is defined as

$$r_k = 1 + n \left(\frac{1}{n} \sum_{l=1}^n \mathbb{I}\{a_k > a_l\} \right) = 1 + n r'_k, \quad k \in [n].$$

To simplify the analysis of the ranking algorithm, we assume that there are no ties: $a_k \neq a_l$ for any $k \neq l$. In the GoRank algorithm (Van Elst et al., 2025a), each node k estimates its rank r_k through a running average combined with a random swapping process. Let $R_k(t)$ and $R'_k(t)$ denote the local estimates of r_k and r'_k , respectively, at node $k \in [n]$ and iteration $t \geq 1$. Define $m = \lfloor \alpha n \rfloor$. For rank-based trimming, our objective is to bound the probability $p_k(t) = \mathbb{P}(|R_k(t) - r_k| \geq \gamma_k)$ where $\gamma_k = \min(|r_k - b_1|, |r_k - b_2|) \geq 1/2$, with $b_1 = m + 1/2$ and $b_2 = n-m+1/2$. As detailed in (Van Elst et al., 2025b), this quantity is central because the estimated weights determining whether to retain each observation or gradient are given by $W_k(t) = \mathbb{I}\{R_k(t) \in I_{n,\alpha}\}$, where $I_{n,\alpha} = [b_1, b_2]$ denotes the inclusion interval. The corresponding true weight is $w_k = \mathbb{I}\{r_k \in I_{n,\alpha}\}$. Taking expectations, we obtain $\mathbb{E}[W_k(t)] = \mathbb{P}(R_k(t) \in I_{n,\alpha})$, which yields

$$|\mathbb{E}[W_k(t)] - w_k| \leq \mathbb{P}(|R_k(t) - r_k| \geq \gamma_k) = p_k(t).$$

Since both $W_k(t)$ and w_k are indicator functions, we also have $\mathbb{E}|W_k(t) - w_k| \leq p_k(t)$. Prior work (Van Elst et al., 2025a;b) derived bounds on $p_k(t)$ via Markov's inequality, using either $\mathbb{E}|R_k(t) - r_k|$ or $\mathbb{E}|R_k(t) - r_k|^2$.

In what follows, we derive bounds on $p_k(t)$ directly using concentration inequalities for Markov chains, exploiting the fact that $R'_k(t)$ can be expressed as an average of dependent samples drawn from a Markov chain. Here, we focus on the synchronous setting. The GoRank update rule yields

$$R'_k(t) = \frac{1}{t} \sum_{s=1}^t f_k(\eta_s), \quad \text{with } f_k(\eta_s) := \mathbb{I}\{a_k > a_{\eta_s(k)}\},$$

and $\eta_s(k)$ denotes the k -th component of the data permutation $\eta_s \in S_n$ at iteration s , which evolves according to the swapping process. Under the stationary distribution,

$$\mathbb{E}_\pi[f_k(\eta)] = \frac{1}{n!} \sum_{\eta \in S_n} \mathbb{I}\{a_k > a_{\eta(k)}\} = r'_k.$$

The permutations $\{\eta_s\}_{s \geq 1}$ are generated by an interchange process on the graph G , which can be modeled as a discrete-time reversible, irreducible, and aperiodic Markov chain with state space S_n (see the appendix E for details). Given sampling probabilities $\mathbf{P} = (p_e)_{e \in E}$, we define the

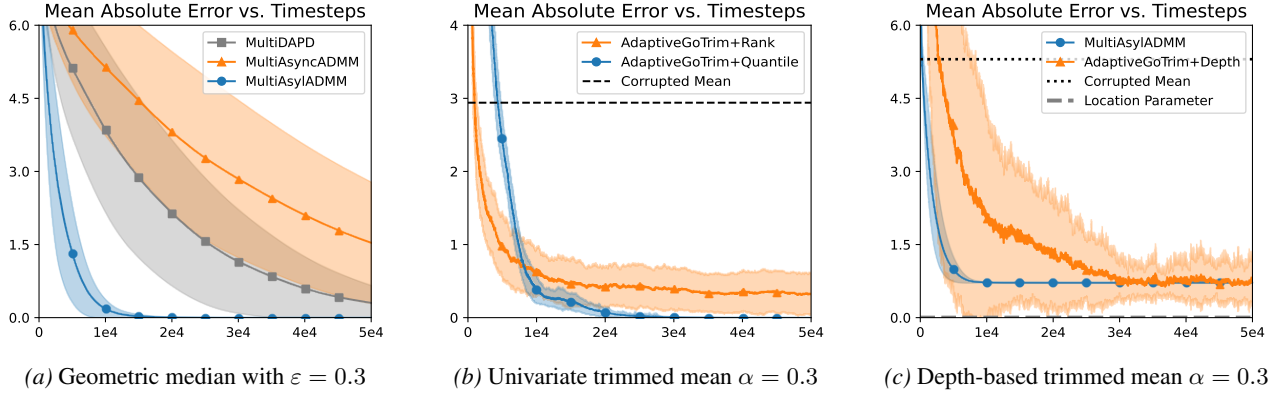


Figure 2. (a) Comparison of different optimization methods on geometric median estimation. (b) Comparison of quantile-based (via AsylADMM) versus rank-based (via GoRank) trimming for robust mean estimation. (c) Comparison of depth-based trimmed means (via GoDepth) with geometric median (via AsylADMM). All plots show mean absolute error versus number of iterations.

weighted graph Laplacian as $\mathbf{L}(\mathbf{P}) = \sum_{e \in E} p_e \mathbf{L}_e$, where $\mathbf{L}_e = (\mathbf{e}_i - \mathbf{e}_j)(\mathbf{e}_i - \mathbf{e}_j)^\top$ is the elementary Laplacian associated with edge $e = (i, j)$. A key result from Caputo et al. (2010) establishes that the spectral gap of the interchange process equals the spectral gap of this weighted graph Laplacian, that is $1 - \lambda_2 = c$ where λ_2 denotes the second-largest eigenvalue of the transition matrix and $c \in (0, 1)$ is the smallest positive eigenvalue of $\mathbf{L}(\mathbf{P})$. This connection allows us to derive a deviation bound in expectation using c as the spectral gap parameter. The inequality stated below can be derived from the Hoeffding’s type probability bound proved by A. León & Perron (2004).

Theorem 4.1 (Exponential Bound). *Under stationary distribution π , for $t \geq 1$, the trimming weight estimated using synchronous GoRank at node k satisfies:*

$$|\mathbb{E}_\pi[W_k(t)] - w_k| \leq 2 \exp\left(-\frac{2}{2-c} \cdot ct\gamma_k^2 n^{-2}\right) ,$$

where c denotes the spectral gap of $\mathbf{L}(\mathbf{P})$ and $\gamma_k = \min(|r_k - b_1|, |r_k - b_2|)$.

The proof is deferred to Appendix E. Additionally, a Bernstein-type tail probability bound, which exploits the variance $V_k = r'_k(1 - r'_k)$, can be derived following the techniques in Paulin (2015), see Appendix E.

Remark 4.2. We point out that, when the initial distribution ν is not equal to the stationary law π , the exponential bound still holds true, up to an additive constant proportional to c^t , see e.g., Isaacson & Madsen (1976).

4.3. Experiments

Here, we present experiments corresponding to the problems introduced in Section 4.1. Unless otherwise specified, we use the same experimental setup as in Section 3.2. The code is available in the supplementary material.

Plot (a). We compare existing optimization methods on geometric median estimation using a 2D contaminated Gaussian with contamination level $\varepsilon = 0.3$; see Appendix F for details. Note that Multi<Method> refers to the same methods as in Section 3, but using the proximal operator of the geometric median (see Appendix D). We observe that AsylADMM outperforms both DAPD and AsyncADMM, consistent with the results for univariate estimation.

Plot (b). We compare rank-based and quantile-based trimming combined with Adaptive GoTrim for trimmed mean estimation, alongside median estimation using AsylADMM. The level of contamination is $\varepsilon = 0.2$ and the trimming parameter $\alpha = 0.3$. We observe that quantile-based trimming with Adaptive GoTrim eventually converges, whereas rank-based trimming converges considerably more slowly. All methods outperform the corrupted mean, showing greater robustness to outliers (i.e., a higher breakdown point).

Plot (c). We investigated the depth-based trimmed mean using trimming parameter $\alpha = 0.3$ with the method described in Section 4.1. We observe strong empirical convergence, though not as fast as the geometric median. Nevertheless, this is an encouraging indication that depth-based trimming is effective and could be applied to more challenging problems like robust optimization. Additional experiments on the convergence of L_2 depth estimation and its corresponding α -quantile estimation are provided in Appendix F.

5. Conclusion

We introduced AsylADMM, a novel asynchronous ADMM-based gossip algorithm for decentralized median and quantile estimation that achieves significant memory efficiency and faster empirical convergence compared to existing methods. We demonstrated its broad applicability through quantile-based trimming, geometric median estimation, and depth-based trimming. Our theoretical contributions, includ-

ing convergence analysis for the synchronous variant and a novel analysis of rank-based trimming, provide a foundation for future work. In Appendix G, we outline a potential approach to proving convergence of AsylADMM using martingale theory and discuss the remaining technical obstacles. In Appendix H, experiments comparing AsylADMM with its synchronous variant show faster convergence per full graph use (*i.e.*, $|E|$ asynchronous updates), confirming the practical efficiency of our method.

Impact Statement

This paper presents work whose goal is to advance the field of Machine Learning. There are many potential societal consequences of our work, none which we feel must be specifically highlighted here.

Acknowledgements

This research was supported by the PEPRA IA Foundry and Hi!Paris ANR Cluster IA France 2030 grants. The authors thank the program for its funding and support.

References

A. León, C. and Perron, F. Optimal hoeffding bounds for discrete reversible markov chains. *The Annals of Applied Probability*, 2004.

Aldous, D. and Fill, J. A. Reversible markov chains and random walks on graphs, 2002. Unfinished monograph, recompiled 2014, available at <http://www.stat.berkeley.edu/\simaldous/RWG/book.html>.

Ayadi, A., Ghorbel, O., Obeid, A. M., and Abid, M. Outlier detection approaches for wireless sensor networks: A survey. *Computer Networks*, 129:319–333, 2017.

Bianchi, P., Hachem, W., and Iutzeler, F. A coordinate descent primal-dual algorithm and application to distributed asynchronous optimization. *IEEE Transactions on Automatic Control*, 61(10):2947–2957, 2015.

Boyd, S., Ghosh, A., Prabhakar, B., and Shah, D. Randomized gossip algorithms. *IEEE transactions on information theory*, 52(6):2508–2530, 2006.

Boyd, S., Parikh, N., Chu, E., Peleato, B., Eckstein, J., et al. Distributed optimization and statistical learning via the alternating direction method of multipliers. *Foundations and Trends® in Machine learning*, 3(1):1–122, 2011.

Caputo, P., Liggett, T., and Richthammer, T. Proof of aldous’ spectral gap conjecture. *Journal of the American Mathematical Society*, 23(3):831–851, 2010.

Duchi, J. C., Agarwal, A., and Wainwright, M. J. Dual averaging for distributed optimization: Convergence analysis and network scaling. *IEEE Transactions on Automatic control*, 57(3):592–606, 2011.

Huber, P. J. and Ronchetti, E. M. *Robust statistics*. John Wiley & Sons, 2011.

Isaacson, D. and Madsen, R. *Markov Chains Theory and Applications*. John Wiley & Sons, 1976.

Iutzeler, F. Distributed computation of quantiles via admm. *IEEE Signal Processing Letters*, 24(5):619–623, 2017.

Iutzeler, F., Bianchi, P., Ciblat, P., and Hachem, W. Asynchronous distributed optimization using a randomized alternating direction method of multipliers. In *52nd IEEE conference on decision and control*, pp. 3671–3676. IEEE, 2013.

Iutzeler, F., Bianchi, P., Ciblat, P., and Hachem, W. Explicit convergence rate of a distributed alternating direction method of multipliers. *IEEE Transactions on Automatic Control*, 61(4):892–904, 2015.

Jalalzai, H., Cléménçon, S., and Sabourin, A. On binary classification in extreme regions. *Advances in Neural Information Processing Systems*, 31, 2018.

Lopuhaä, H. P. and Rousseeuw, P. J. Breakdown points of affine equivariant estimators of multivariate location and covariance matrices. *The Annals of Statistics*, pp. 229–248, 1991.

Minsker, S. Geometric median and robust estimation in banach spaces. *Bernoulli*, 2015.

Mosler, K. Depth statistics. *Robustness and complex data structures: Festschrift in Honour of Ursula Gather*, pp. 17–34, 2013.

Nedic, A. and Ozdaglar, A. Distributed subgradient methods for multi-agent optimization. *IEEE Transactions on automatic control*, 54(1):48–61, 2009.

Oja, H. *Multivariate Median*, pp. 3–15. Springer Berlin Heidelberg, Berlin, Heidelberg, 2013. ISBN 978-3-642-35494-6. doi: 10.1007/978-3-642-35494-6_1. URL https://doi.org/10.1007/978-3-642-35494-6_1.

Oosterhoff, J. Trimmed mean or sample median? *Statistics & Probability Letters*, 20(5):401–409, 1994.

Parikh, N., Boyd, S., et al. Proximal algorithms. *Foundations and trends® in Optimization*, 1(3):127–239, 2014.

Paulin, D. Concentration inequalities for markov chains by marton couplings and spectral methods. *Electronic journal of probability*, 2015.

Serfling, R. Depth functions in nonparametric multivariate inference. *DIMACS Series in Discrete Mathematics and Theoretical Computer Science*, 72:1, 2006.

Shi, W., Ling, Q., Yuan, K., Wu, G., and Yin, W. On the linear convergence of the admm in decentralized consensus optimization. *IEEE Transactions on Signal Processing*, 62(7):1750–1761, 2014.

Shi, W., Ling, Q., Wu, G., and Yin, W. A proximal gradient algorithm for decentralized composite optimization. *IEEE Transactions on Signal Processing*, 63(22):6013–6023, 2015.

Van Elst, A., Colin, I., and Cléménçon, S. Asynchronous gossip algorithms for rank-based statistical methods. *To appear in International Conference on Federated Learning Technologies and Applications (FLTA)*, 2025a.

Van Elst, A., Colin, I., and Cléménçon, S. Robust distributed estimation: Extending gossip algorithms to ranking and trimmed means. *To appear in the Proceedings of Advances in Neural Information Processing Systems (NeurIPS)*, 2025b.

Wasserman, L. *All of statistics: a concise course in statistical inference*. Springer Science & Business Media, 2013.

Wei, E. and Ozdaglar, A. Distributed alternating direction method of multipliers. In *2012 IEEE 51st IEEE Conference on Decision and Control (CDC)*, pp. 5445–5450. IEEE, 2012.

Wei, E. and Ozdaglar, A. On the $o(1/k)$ convergence of asynchronous distributed alternating direction method of multipliers, 2013. URL <https://arxiv.org/abs/1307.8254>.

Yang, Y., Guan, X., Jia, Q.-S., Yu, L., Xu, B., and Spanos, C. J. A survey of admm variants for distributed optimization: Problems, algorithms and features. *arXiv preprint arXiv:2208.03700*, 2022.

Table of contents

Appendix A details the existing optimization algorithms for quantile estimation discussed in Section 2. Appendix B presents the convergence analysis for the synchronous variant. Appendix C provides additional experiments that support the discussion in Section 3.3. Appendix D describes algorithms and details from Section 4.1. Appendix E includes theoretical results supporting the claims in Section 4.2. Appendix F provides additional experiments for Section 4.3. Appendix G outlines the technical challenges involved in the convergence analysis of AsyADMM. Appendix H provides an empirical comparison using the synchronous variant. Appendix I provides empirical results on robust regression via trimming.

A. Existing Optimization Methods for Quantile Estimation

In this section, we describe the baseline algorithms used in our comparative experiments in Section 3.3.

A.1. Distributed Subgradient Descent from Nedic & Ozdaglar (2009)

Algorithm 3 Subgradient Descent

- 1: **Input:** Initial vectors a_1, \dots, a_n ; step size $\rho > 0$, subgradient of pinball loss g .
- 2: **Initialization:** For all nodes $k = 1, \dots, n$: $x_k \leftarrow a_k$, $\mu_k \leftarrow 0$.
- 3: **for** $t = 0, 1, \dots$ **do**
- 4: For all k , update: $x_k^+ \leftarrow x_k - \frac{\rho}{\sqrt{t+1}} g_k$.
- 5: Draw $e = (i, j) \in E$ with probability p_e and compute average: $x_i^+, x_j^+ \leftarrow \frac{1}{2}(x_i^+ + x_j^+)$.
- 6: **end for**

A.2. AsyncADMM from Iutzeler et al. (2013)

Algorithm 4 Async-ADMM

- 1: **Input:** Initial vectors a_1, \dots, a_n ; step size $\rho > 0$.
- 2: **Initialization:** For all agents $k = 1, \dots, n$: $x_k \leftarrow a_k$, $\lambda_{kl} \leftarrow 0$, $\bar{x}_{kl} \leftarrow a_k$ for all $l \in \mathcal{N}_k$.
- 3: **for** $t = 0, 1, \dots$ **do**
- 4: Draw $(i, j) \in E$ with probability p_{ij} .
- 5: Agents $k \in \{i, j\}$ update their primal variable: $x_k \leftarrow \text{prox}_{\frac{f_k}{\rho d_k}} \left(\frac{1}{d_k} (\sum_{l \in \mathcal{N}_k} \bar{x}_{kl} - \lambda_{kl}) \right)$
- 6: Compute average: $\bar{x} \leftarrow \frac{x_i + x_j}{2}$.
- 7: Update: $\lambda_{ij} \leftarrow \lambda_{ij} + \rho(x_i - \bar{x})$; $\lambda_{ji} \leftarrow \lambda_{ji} + \rho(x_j - \bar{x})$.
- 8: Update $\bar{x}_{ij}, \bar{x}_{ji} \leftarrow \bar{x}$.
- 9: **end for**

A.3. DADP with $f = 0$ from Bianchi et al. (2015)

Algorithm 5 DADP (adapted for $f = 0$ using $\tau = \rho/2$ and $\rho \mapsto 1/\rho$)

- 1: **Input:** Initial vectors a_1, \dots, a_n ; step size $\rho > 0$.
- 2: **Initialization:** For all agents $k = 1, \dots, n$: $x_k \leftarrow a_k$, $\lambda_{kl} \leftarrow 0$, $\bar{x}_{kl} \leftarrow a_k$ for all $l \in \mathcal{N}_k$.
- 3: **for** $t = 0, 1, \dots$ **do**
- 4: Draw $(i, j) \in E$ with probability p_{ij} .
- 5: Update dual variables:

$$\lambda_{ij} \leftarrow \frac{1}{2}(\lambda_{ij} - \lambda_{ji}) + \frac{\rho}{2}(x_i - x_j); \lambda_{ji} \leftarrow -\lambda_{ij}.$$
- 6: Agents $k \in \{i, j\}$ update their primal variable:

$$x_k \leftarrow \text{prox}_{\frac{f_k}{\rho d_k}} \left(\frac{1}{2}x_k + \frac{1}{2d_k} \sum_{l \in \mathcal{N}_k} (\bar{x}_{kl} - \frac{1}{\rho} \lambda_{kl}) \right).$$
- 7: Update neighbor values: $\bar{x}_{ij} \leftarrow x_j$, $\bar{x}_{ji} \leftarrow x_i$.
- 8: **end for**

B. Convergence Analysis of the Synchronous Variant

In this section, we provide useful theoretical results for the convergence analysis of the synchronous variant.

B.1. Additional Details

The algorithm outlined in Algorithm 1 corresponds to a reordered variant of ADMM that updates variables in the sequence (z, y, x) rather than the standard (x, z, y) ordering:

$$\begin{aligned} z^{t+1} &:= \arg \min_z \left(g(z) + \frac{\rho}{2} \|z - Mx^t + y^t/\rho\|^2 \right), \\ y^{t+1} &:= y^t + \rho(z^{t+1} - Mx^t) \\ x^{t+1} &:= \arg \min_x \left(f(x) + \frac{\rho}{2} \|z^{t+1} - Mx + y^{t+1}/\rho\|^2 \right). \end{aligned}$$

We now verify that the z -update reduces to the averaging step in our algorithm. Recall that $g_e(z_e) = \iota_C(z_e)$ is the convex indicator function for $C = \text{span}(\mathbf{1}_2)$. Since the objective is separable across edges, the minimization decomposes into independent subproblems, each solved by orthogonal projection onto C . Consider edge $e = (i, j)$, and let $x_e = (x_i, x_j)$ and $y_e = (y_{e,i}, y_{e,j})$. The z -update becomes:

$$z_e^{t+1} = \Pi_C (x_e^t - y_e^t/\rho) := \arg \min_{z \in C} \|z - (x_e^t - y_e^t/\rho)\|^2.$$

The projection onto $\text{span}(\mathbf{1}_2)$ yields $z_e = \bar{x}\mathbf{1}_2$ with $\bar{x} = (x_i + x_j)/2$. This follows from the antisymmetry of the dual variables, which ensures $(y_{e,i} + y_{e,j})/2 = 0$.

B.2. Proof of Lemma 3.1

We establish the equivalence of the following two statements:

- (a) $x_k \in \operatorname{argmin}_{x_k} \mathcal{L}_\rho^{(k)}(x_k, z_k, y_k)$ where $z_k = (z_e)_{e \in N_k}$ and $y_k = (y_{e,k})_{e \in N_k}$;
- (b) $x_k = \operatorname{prox}_{f_k/(\rho d_k)}(\hat{z}_k + \hat{\mu}_k/\rho)$, where $\hat{z}_k = \mathbf{1}_{d_k}^\top z_k/d_k$ and $\hat{\mu}_k = \mathbf{1}_{d_k}^\top y_k/d_k$.

Expanding the augmented Lagrangian, we have

$$\mathcal{L}_\rho^{(k)}(x_k, z_k, y_k) = f_k(x_k) + \sum_{e \in N_k} \left(y_{e,k}^\top (z_e - x_k) + \frac{\rho}{2} \|x_k\|^2 - \rho z_e^\top x_k + \frac{\rho}{2} \|z_e\|^2 \right).$$

Since we minimize over x_k , terms independent of x_k can be discarded. The optimization problem thus reduces to

$$f_k(x_k) + \sum_{e \in N_k} \left(\frac{\rho}{2} \|x_k\|^2 - (y_{e,k} + \rho z_e)^\top x_k \right).$$

Substituting the definitions of \hat{z}_k and $\hat{\mu}_k$, and factoring out $\rho d_k/2$, we obtain $f_k(x_k) + \frac{\rho d_k}{2} \left(\|x_k\|^2 - 2(\hat{z}_k + \hat{\mu}_k/\rho)^\top x_k \right)$. Letting $u = \hat{z}_k + \hat{\mu}_k/\rho$ and completing the square yields

$$\operatorname{prox}_{\frac{f_k}{\rho d_k}}(u) := \operatorname{argmin}_x \left\{ f_k(x) + \frac{\rho d_k}{2} \|u - x\|^2 \right\},$$

which completes the proof. \square

B.3. Proof of Inequality I

We aim to establish that $f(x^{t+1}) - f(x^*) \leq \rho (M\tilde{x}^{t+1} - y^{t+1})^\top r^{t+1}$. Recall that the dual update takes the form $y^{t+1} = y^t + \rho(z^{t+1} - Mx^t)$. We begin by analyzing the z -update. The optimality condition yields $0 \in \partial g_e(z_e^{t+1}) + \rho(z_e^{t+1} - x_e^t + y_e^t/\rho)$. Substituting the dual update $y_e^{t+1} = y_e^t + \rho(z_e^{t+1} - x_e^t)$, this simplifies to $0 \in \partial g_e(z_e^{t+1}) + y_e^{t+1}$, or equivalently, $-y_e^{t+1} \in \partial g_e(z_e^{t+1})$. Applying the subgradient inequality, we obtain $g_e(z_e^{t+1}) - g_e(z_e^*) \leq - (y_e^{t+1})^\top (z_e^{t+1} - z_e^*)$. Summing over all edges:

$$g(z^{t+1}) - g(z^*) \leq - \sum_k \sum_{e \in N_k} y_{e,k}^{t+1}^\top (z_e^{t+1} - z_e^*). \quad (4)$$

Next, we analyze the x -update. The optimality condition for the proximal operator yields, for $k, 0 \in \partial f_k(x_k^{t+1}) + \rho d_k(x_k^{t+1} - u)$, where $u := \hat{z}_k^{t+1} + \hat{\mu}_k^{t+1}/\rho$. Observing that $\rho(x_k^{t+1} - u) = -(\rho r_k^{t+1} + \hat{\mu}_k^{t+1})$, and applying the subgradient inequality, we obtain $f_k(x_k^{t+1}) - f_k(x_k^*) \leq d_k(\rho r_k^{t+1} + \hat{\mu}_k^{t+1})^\top (x_k^{t+1} - x_k^*)$. Summing over all $k \in [n]$ and expressing the result in terms of the original edge variables z_e and $y_{e,k}$, we have

$$f(x^{t+1}) - f(x^*) \leq \sum_k \left(\sum_{e \in N_k} \rho(z_e^{t+1} - x_k^{t+1}) + y_{e,k}^{t+1} \right)^\top (x_k^{t+1} - x_k^*). \quad (5)$$

Adding Equation (4) and Equation (5) and using the facts that, by construction, $g(z) = 0$ and $Mx^* = z^*$, we arrive at

$$f(x^{t+1}) - f(x^*) \leq \sum_k \left(\sum_{e \in N_k} \rho \tilde{x}_k^{t+1} - y_{e,k}^{t+1} \right)^\top r_{e,k}^{t+1}.$$

Rewriting in matrix form establishes the desired inequality. \square

B.4. Proof of Inequality II

We now establish inequality $f(x^*) - f(x^{t+1}) \leq y^*^\top r^{t+1}$. We first recall the main assumption.

Assumption B.1. The unaugmented Lagrangian \mathcal{L}_0 has a saddle point. Specifically, there exists (x^*, z^*, y^*) such that

$$\mathcal{L}_0(x^*, z^*, y) \leq \mathcal{L}_0(x^*, z^*, y^*) \leq \mathcal{L}_0(x, z, y^*)$$

holds for all (x, z, y) .

Since (x^*, z^*, y^*) is a saddle point of \mathcal{L}_0 , we have $\mathcal{L}_0(x^*, z^*, y^*) \leq \mathcal{L}_0(x^{t+1}, z^{t+1}, y^*)$. Expanding both sides and using $Mx^* = z^*$, we obtain the desired inequality. \square

C. Additional Experiments for Section 3.3

This section presents additional experiments and ablation studies for Section 3.3.

C.1. Impact of Network Size using Setup of Plot (a)

Here, we investigate the impact of network size on various graph topologies under the experimental setup of Plot (a) from section 3.3.

In Figure 3, we compared the optimization methods on different graph topologies with different network sizes. First, we consider small networks with $n = 21$. Notably, DAPD and AsyncADMM do not converge well on the complete graph. While this may seem surprising given that the complete graph has the best connectivity, it likely stems from both methods' reliance on outdated information, which becomes problematic when nodes have many neighbors. The complete graph may also be inherently harder for ADMM-like algorithms due to the larger number of constraints. On the Watts-Strogatz graph, there is almost no difference between DAPD, Asyl-ADMM, and AsyncADMM. This can be explained by the low average degree (equal to 4), so the outdated information issue does not play a significant role.

Then, we repeat the experiment with $n = 101$. All three methods show similar convergence on the cycle graph, which is unsurprising given that it has the lowest average degree of 2.

Finally evaluate our algorithm on large-scale networks (with $n = 501$ and $n = 1001$ nodes). For these experiments, we reduced the range of ρ to $(0.01, 0.1)$. AsylADMM demonstrates even stronger competitive performance relative to the baseline algorithms, achieving consistent fast convergence on both Geometric and Watts-Strogatz topologies.

C.2. Impact of α -level on quantile Estimation using Setup of Plot (b)

Here, we investigate how varying the quantile level α affects the convergence of the optimization algorithms under the experimental setup described in Section 3.3, Plot (b).

The results in Figure 4 indicate that the algorithms show some sensitivity to the choice of α , with degraded performance at extreme quantiles such as $\alpha = 0.1$ and $\alpha = 0.9$. This behavior can be attributed to contamination in the tails of the

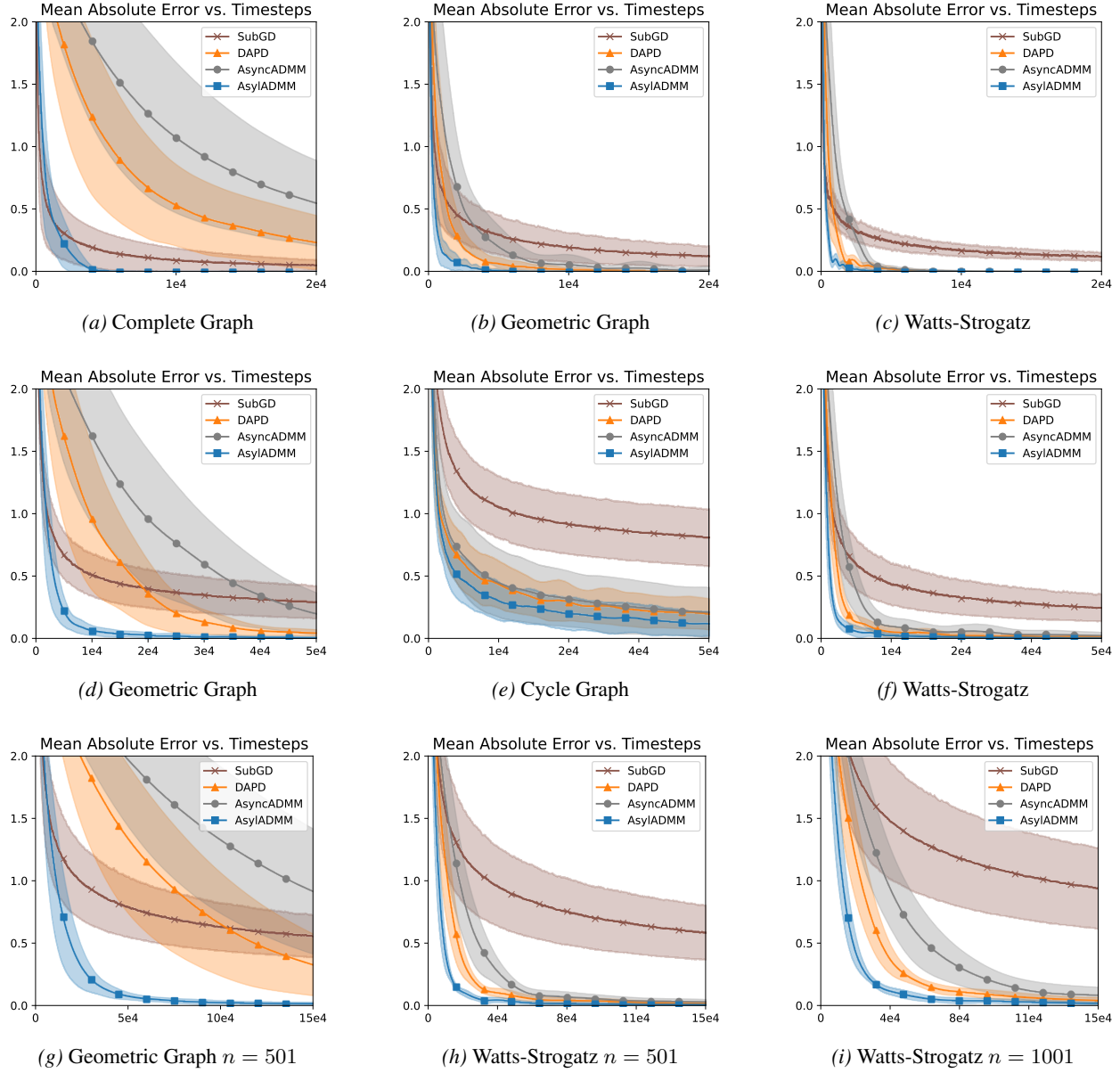


Figure 3. Setup is the same as Plot (a) in Section 3 with different network sizes. In Plot (a), (b), and (c), we take $n = 21$. In Plot (d), (e), and (f), we take $n = 101$. In plot (g), (h), (i), the size is specified in the caption.

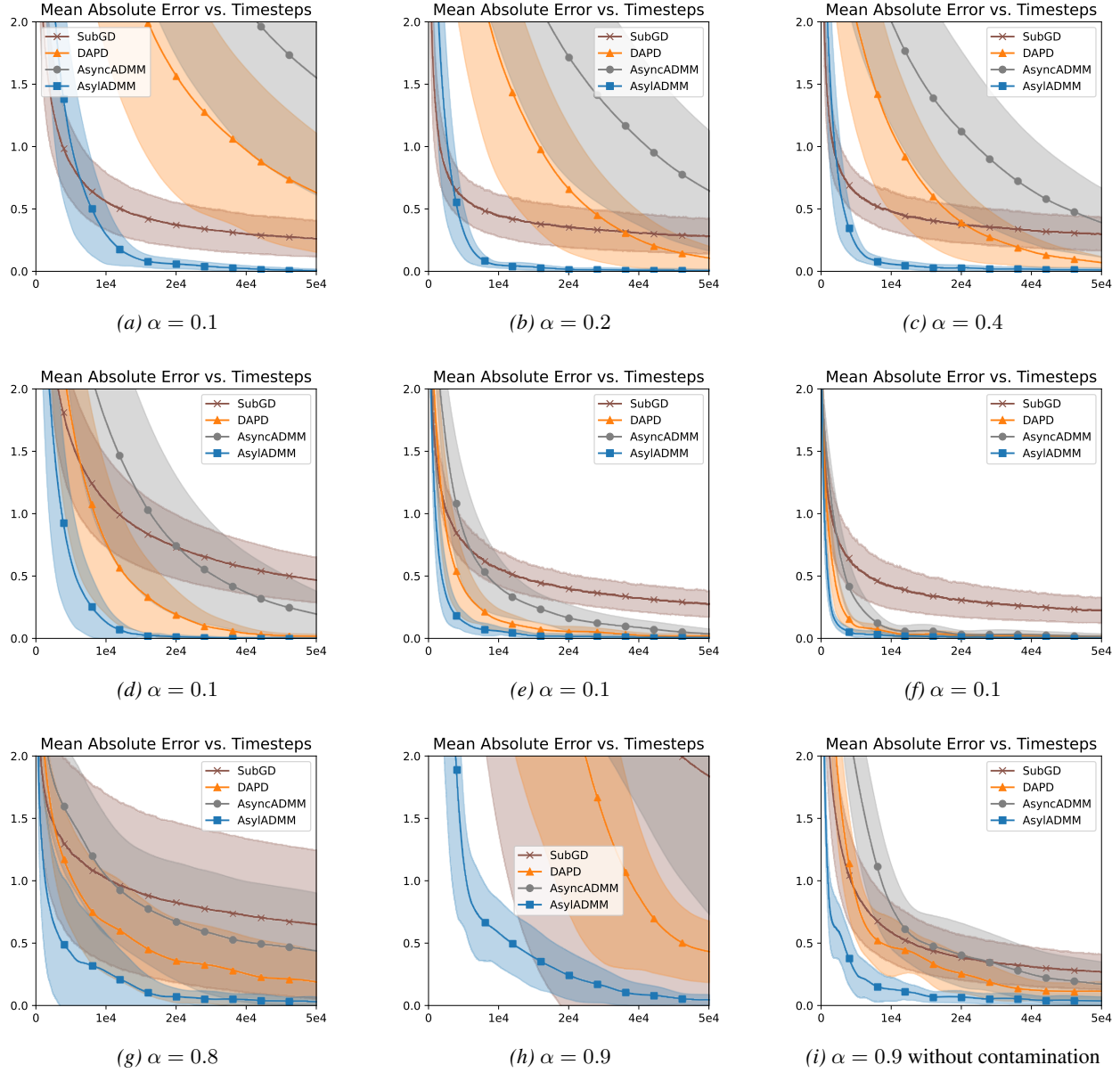


Figure 4. Setup is the same as plot (b) in Section 3 with $n = 101$ nodes on various graph topologies. Plots (a), (b), and (c) use a Geometric graph. Plots (d), (e), and (f) use a Watts-Strogatz. Plots (g), (h), and (i) use a Geometric graph.

distribution. Performance degradation is particularly pronounced for high quantiles, which is consistent with the fact that the chosen contamination scheme primarily affects large values (see Plot (h)). Indeed, removing the data contamination yields more stable convergence (see Plot (i)). Overall, AsylADMM demonstrates robust performance across varying α levels and under data contamination, outperforming the baseline methods, particularly at high quantiles in the presence of contaminated data.

C.3. Impact of Distribution with Setup of Plot (c)

Here, we investigate how the choice of distribution and its contamination level affect convergence using the setup of Plot (c) from section 3.3.

From Figure 5, we observe that AsylADMM converges quickly across most topologies when the data is not contaminated. Increasing the contamination level to $\varepsilon = 0.4$ makes convergence significantly harder, which is not surprising, but the algorithm still eventually converges. We then examine the Cauchy distribution with the same location parameter as the standard Gaussian and the same scale as the Gaussian in the contaminated portion. We choose this example because the Cauchy is a classic “pathological distribution” in statistics—both its expected value and variance are undefined—which makes the median all the more relevant. Here again, we observe that the algorithm converges well.

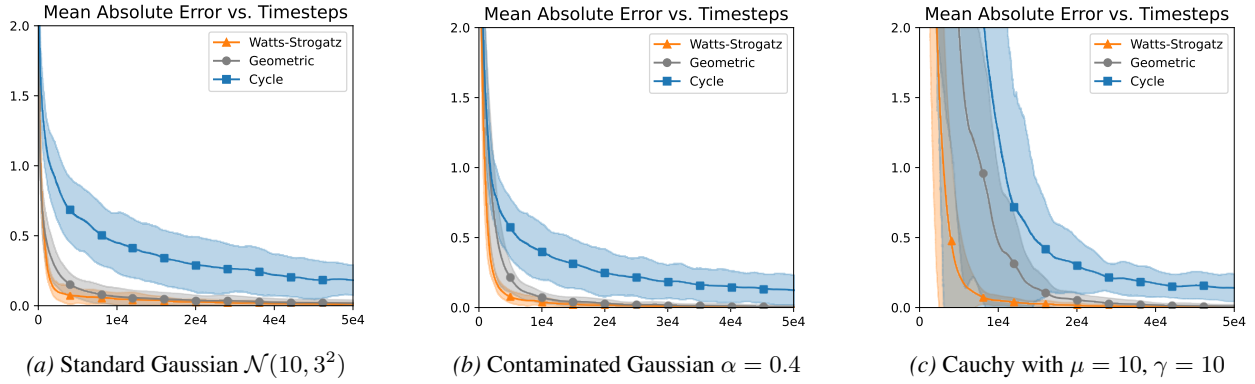


Figure 5. We use the same setup as in plot (c) of Section 3, varying only the data distribution.

D. Additional Algorithms and Details for Section 4.1

D.1. Geometric Median

Consider a decentralized geometric median problem. Each agent $i \in \{1, \dots, n\}$ holds a vector $a_i \in \mathbb{R}^d$, and all the agents collaboratively calculate the geometric median $x \in \mathbb{R}^d$ of all a_i . This task can be formulated as solving the following minimization problem:

$$\min_{x \in \mathbb{R}^d} \frac{1}{n} \sum_{i=1}^n \|x - a_i\|_2.$$

First, we recall the proximal operator for the Euclidean norm; see section 6.5.1 in Parikh et al. (2014). Let $g = \|\cdot\|_2$, the Euclidean norm in \mathbb{R}^d . The corresponding proximal operator is given by

$$\text{prox}_{\lambda g}(v) = (1 - \lambda/\|v\|_2)_+ v = \begin{cases} (1 - \lambda/\|v\|_2) v & \|v\|_2 \geq \lambda \\ 0 & \|v\|_2 < \lambda. \end{cases}$$

From section 2.2 in Parikh et al. (2014), we can use the precomposition property for $f_i(x) = \|x - a_i\|_2 = g(x - a_i)$ to obtain $\text{prox}_{\lambda f_i}(v) = a_i + \text{prox}_{\lambda g}(v - a_i)$.

D.2. Algorithm: GoRank

Algorithm 6 Asynchronous GoRank

```

1: Init: For each  $k \in [n]$ ,  $Y_k \leftarrow X_k$ ,  $R'_k \leftarrow 0$ ,  $C_k \leftarrow 1$ .
2: for  $t = 0, 1, \dots$  do
3:   Draw  $e = (i, j) \in E$  with probability  $p_e > 0$ .
4:   for  $k \in \{i, j\}$  do
5:     Set  $R'_k \leftarrow (1 - 1/C_k) R'_k + (1/C_k) \mathbb{I}_{\{X_k > Y_k\}}$ .
6:     Update rank estimate:  $R_k \leftarrow nR'_k + 1$ .
7:     Set  $C_k \leftarrow C_k + 1$ .
8:   end for
9:   Swap auxiliary observation:  $Y_i \leftrightarrow Y_j$ .
10: end for

```

Algorithm 7 Synchronous GoRank.

```

1: Init: For each  $k \in [n]$ , initialize  $Y_k \leftarrow X_k$  and  $R'_k \leftarrow 0$ . // init(k)
2: for  $s = 1, 2, \dots$  do
3:   for  $k = 1, \dots, n$  do
4:     Update estimate:  $R'_k \leftarrow (1 - 1/s) R'_k + (1/s) \mathbb{I}_{\{X_k > Y_k\}}$ .
5:     Update rank estimate:  $R_k \leftarrow nR'_k + 1$ . // update(k, s)
6:   end for
7:   Draw  $(i, j) \in E$  uniformly at random.
8:   Swap auxiliary observation:  $Y_i \leftrightarrow Y_j$ . // swap(i, j)
9: end for
10: Output: Estimate of ranks  $R_k$ .

```

D.3. Algorithm: Adaptive GoTrim

We adapt the Adaptive GoTrim algorithm presented in [Van Elst et al. \(2025a\)](#) to include the quantile-based rule. The trimming rule trim corresponds to the chosen algorithm (either GoRank or AsyLADMM) and its associated weight rule. The function `init` handles algorithm initialization, `update` performs the local update step, and `exchange` executes the communication step in the gossip protocol (either averaging or swapping). The function `estimate` applies the appropriate weight function: for quantile-based trimming, $W_k(t) = \mathbb{I}\{X_k \in [q_k^\alpha(t), q_k^{1-\alpha}(t)]\}$, while for rank-based trimming, $W_k(t) = \mathbb{I}\{R_k(t) \in I_{n,\alpha}\}$.

D.4. Algorithm: Regression with Gradient Trimming

For robust regression, we employ decentralized gradient descent with gradient trimming. Since the gradient at node i is essentially proportional to $d_i = \|x_i\| \cdot |y_i|$, we compute the trimming rules based on d_1, \dots, d_n and exclude from the local update any gradient whose node contains an d_i outside the authorized range. This approach is similar to what is done in extreme value theory in which the k largest datapoints according to a chosen metric are considered extreme and to be dealt differently than the rest of the dataset ([Jalalzai et al., 2018](#)). Moreover, these arbitrarily large gradients can make the optimization process less stable. This approach reduces to estimating the α -quantile of the scores $\{d_i\}_{i=1}^n$. For node k , we include its gradient contribution if $d_k > q_\alpha$, yielding the selection variable $b_k = \mathbb{I}\{d_k > q_\alpha\}$. The resulting algorithm is presented below, where g_k denotes the standard gradient of the linear regression loss evaluated at node k using local data (x_k, y_k) and the current parameter estimate θ_t .

We consider two implementation strategies: *sequential* and *simultaneous*. The sequential approach proceeds in two phases. In the first phase, we estimate the trimming variables $\{b_k\}_{k=1}^n$ until sufficient precision is achieved. In the second phase, we perform optimization with the selection variables fixed. This requires a predetermined number of estimation steps for the first phase 1.

The simultaneous approach estimates $\{b_k\}_{k=1}^n$ concurrently with the optimization iterates. This eliminates the need for predetermined number of estimation steps. However, the selection rule must account for estimation uncertainty through an additive correction term $\delta_k(t) = \kappa / \sqrt{c_k(t)}$ where $c_k(t)$ denotes the cumulative number of updates performed by node k up to iteration t , and $\kappa > 0$ is a tunable parameter depending on the graph topology and initial data distribution. Note

Algorithm 8 Adaptive GoTrim

```

1: Input: Trimming level  $\alpha \in (0, 1/2)$ , choice of trimming rule  $\text{trim}$  (e.g., rank-based or quantile-based).
2: Init:  $\forall k, Z_k \leftarrow 0, W_k \leftarrow 0$  and  $R_k \leftarrow \text{trim.init}(k)$ .
3: for  $t = 1, 2, \dots$  do
4:   Draw  $e = (i, j) \in E$  with probability  $p_e > 0$ .
5:   for  $k \in \{i, j\}$  do
6:     Update rank:  $R_k \leftarrow \text{trim.update}(k, t)$ .
7:     Set  $W'_k \leftarrow \text{trim.estimate}(k, t)$ .
8:     Set  $N_k \leftarrow N_k + (W'_k - W_k) \cdot X_k$ .
9:     Set  $M_k \leftarrow M_k + (W'_k - W_k)$ 
10:    Set  $W_k \leftarrow W'_k$ .
11:   end for
12:   Set  $N_i, N_j \leftarrow (N_i + N_j)/2$ .
13:   Set  $M_i, M_j \leftarrow (M_i + M_j)/2$ .
14:   Swap auxiliary variables:  $\text{trim.exchange}(i, j)$ 
15: end for
16: Output: Estimate of trimmed mean  $N_k / \max(1, M_k)$ .

```

that κ may be hard to tune in a decentralized setting and requires further investigation. As estimation precision improves, $\delta_k(t) \rightarrow 0$. The modified inclusion rules become: $R_k(t) > m + \delta_k(t)$ when rank-based and $d_k(t) > q_\alpha(t) + \delta_k(t)$ when quantile-based.

Algorithm 9 Gradient Descent with Gradient Trimming

```

1: Input: Initial vectors  $a_1, \dots, a_n$ ; step size  $\rho > 0, \dots$ 
2: Initialization: For all nodes  $k = 1, \dots, n$ :  $x_k \leftarrow a_k, \mu_k \leftarrow 0$ .
3: for  $t = 0, 1, \dots$  do
4:   For all  $k$ , update:
5:      $b_k \leftarrow \text{trimming\_rule}(k)$ 
6:      $\theta_k^+ \leftarrow \theta_k - \rho b_k g_k$ .
7:   Draw  $e = (i, j) \in E$  with probability  $p_e$  and compute average:  $\theta_i^+, \theta_j^+ \leftarrow \frac{1}{2}(\theta_i^+ + \theta_j^+)$ .
8: end for

```

D.5. Analysis of Quantile-based Trimming

Denote $q_1 = q^\alpha$ and $q_2 = q^{1-\alpha}$ with their corresponding estimates at node k and iteration t , $q_1(t) = q_k^\alpha(t)$ and $q_2(t) = q_k^{1-\alpha}(t)$. We now analyze the conditions under which the estimated weights $W_k(t) = \mathbb{I}\{q_1(t) \leq X_k \leq q_2(t)\}$ differ from their true weights $w_k = \mathbb{I}\{q_1 \leq X_k \leq q_2\}$. Let $\epsilon_1(t) = |q_1(t) - q_1|$ and $\epsilon_2(t) = |q_2(t) - q_2|$ denote the estimation errors of the quantiles, and let $d_1 = |X_k - q_1|$ and $d_2 = |X_k - q_2|$ denote the distances from X_k to the boundary quantiles. A disagreement $W_k(t) \neq w_k$ can only occur when X_k falls within an $\epsilon_j(t)$ -neighborhood of at least one boundary, i.e., $W_k(t) \neq w_k$ implies $X_k \in B(q_1, \epsilon_1(t)) \cup B(q_2, \epsilon_2(t))$. Applying the union bound yields

$$\mathbb{E}|W_k(t) - w_k| = \mathbb{P}(W_k(t) \neq w_k) \leq \mathbb{P}(d_1 \leq \epsilon_1(t)) + \mathbb{P}(d_2 \leq \epsilon_2(t)).$$

Thus, the probability of error is controlled by the estimation errors $\epsilon_1(t)$ and $\epsilon_2(t)$ combined with the distance of X_k to the trimming quantiles.

D.6. Analysis of Rank-based Trimming

The analysis directly follows from Lemma 1 in [Van Elst et al. \(2025b\)](#).

Recall $I_{n,\alpha} = [a, b]$ and define

$$\gamma_k = \begin{cases} \min(b - r_k, r_k - a), & \text{if } a \leq r_k \leq b, \\ a - r_k, & \text{if } r_k < a, \\ r_k - b, & \text{if } r_k > b. \end{cases}$$

Observe that $\gamma_k \geq \frac{1}{2}$ since r_k is always discrete. We now analyze the three different cases. Case 1: $a \leq r_k \leq b$. Then, $|p_k(t) - \mathbb{I}_{\{r_k \in I_{n,\alpha}\}}| = |1 - p_k(t)| = \mathbb{P}(R_k(t) \notin I_{n,\alpha})$. Since we have $\mathbb{P}(|R_k(t) - r_k| \leq \gamma_k) \leq \mathbb{P}(R_k(t) \in I_{n,\alpha})$, it follows that the probability can be upper-bounded as $\mathbb{P}(R_k(t) \notin I_{n,\alpha}) \leq \mathbb{P}(|R_k(t) - r_k| > \gamma_k) \leq \mathbb{P}(|R_k(t) - r_k| \geq \gamma_k)$. Case 2: $r_k < a$. Here, $|p_k(t) - \mathbb{I}_{\{r_k \in I_{n,\alpha}\}}| = p_k(t) = \mathbb{P}(R_k(t) \in I_{n,\alpha})$. Since it holds that $\mathbb{P}(|R_k(t) - r_k| < \gamma_k) \leq \mathbb{P}(R_k(t) \notin I_{n,\alpha})$, we obtain $\mathbb{P}(R_k(t) \in I_{n,\alpha}) \leq \mathbb{P}(|R_k(t) - r_k| \geq \gamma_k)$. Case 3: $r_k > b$. This case follows symmetrically from the previous one. In all cases, we have $|\mathbb{P}(R_k(t) \in I_{n,\alpha}) - \mathbb{I}_{\{r_k \in I_{n,\alpha}\}}| \leq \mathbb{P}(|R_k(t) - r_k| \geq \gamma_k)$.

D.7. Estimation of Data Depths and its α -Quantile

Algorithm 10 Asynchronous GoDepth (L2 Depth)

```

1: Init: For each  $k \in [n]$ ,  $\mathbf{y}_k \leftarrow \mathbf{x}_k$ ,  $z_k \leftarrow 0$ ,  $c_k \leftarrow 1$ .
2: for  $t = 0, 1, \dots$  do
3:   Draw  $e = (i, j) \in E$  with probability  $p_e > 0$ .
4:   Swap auxiliary observations:  $\mathbf{y}_i \leftrightarrow \mathbf{y}_j$ .
5:   for  $k \in \{i, j\}$  do
6:     Set  $c_k \leftarrow c_k + 1$ .
7:     Set  $z_k \leftarrow (1 - 1/c_k) z_k + (1/c_k) \|\mathbf{x}_k - \mathbf{y}_k\|$ .
8:     Update depth estimate:  $d_k \leftarrow 1/(1 + z_k)$ .
9:   end for
10:  end for

```

Algorithm 11 AsyIADMM+GoDepth: estimation of α -quantile of data depths

```

1: Input: Initial vectors  $a_1, \dots, a_n$ ; step size  $\rho > 0$ .
2: Initialization: For all nodes  $k = 1, \dots, n$ :
3:    $\text{godepth.init}(k)$ ;  $\text{asyladmm.init}(k)$ .
4: for  $t = 0, 1, \dots$  do
5:   Draw  $e = (i, j) \in E$  with probability  $p_e$ .
6:   for  $k \in \{i, j\}$  do
7:      $d_k \leftarrow \text{godepth.update}(k)$  // Standard update
8:      $x_k \leftarrow \text{asyladmm.update}(k, d_k)$  // Update using new depth estimate  $d_k$  instead of  $a_k$ 
9:   end for
10:  end for

```

E. Theoretical Results for Section 4.2

This section provides the theoretical results for rank-based trimming. We first describe the properties of the interchange process, then leverage these results to derive concentration bounds for GoRank estimates.

E.1. Properties and Spectral Gap of the Interchange Process

Here, we establish the key properties of the interchange process, and show how its spectral gap can be computed explicitly. The goal is to study concentration properties of the empirical mean $\frac{1}{t} \sum_{s=1}^t f(\eta_s)$, where the samples are dependent permutations generated by an interchange process. The interchange process on the graph G is modeled by a discrete-time reversible Markov chain with state space S_n , the set of permutations of V . The process evolves as follows: from a state $\eta \in S_n$, a transition to state η^{ij} occurs with probability p_{ij} for edge $(i, j) \in E$, where this transition swaps (interchanges) the observations at nodes i and j while keeping the rest of the graph unchanged. Formally, with probability p_{ij} , we have $\eta^{ij} = \eta \circ \tau_{ij}$, where τ_{ij} denotes the transposition of i and j .

We first introduce a lemma characterizing the properties of the Markov chain of the interchange process.

Lemma E.1. *Assume the graph G is connected and non-bipartite. Then, the Markov chain of the interchange process on the graph G is irreducible and aperiodic, and has the uniform distribution as its stationary distribution. Moreover, the chain is reversible.*

Proof. The irreducibility and aperiodicity follow from the assumption that the graph G is connected and non-bipartite. Since the state space S_n is finite, the chain converges to a unique stationary distribution π satisfying $\pi = \pi\mathbf{P}$, where \mathbf{P} denotes the transition matrix. By symmetry of the edge weights ($p_{ij} = p_{ji}$), the transition matrix is doubly stochastic, meaning the uniform distribution $\pi(\sigma) = 1/n!$ for all $\sigma \in S_n$ is a left eigenvector of \mathbf{P} with eigenvalue 1. The reversibility of the chain follows from the symmetry of the edge weights. \square

Now, we state a result on the spectral gap of the interchange process.

Lemma E.2. *The spectral gap of the interchange process is equal to the spectral gap of the Laplacian of the weighted graph, that is, $\gamma^{IP} := 1 - \lambda = c$, where λ is the second-largest eigenvalue of the transition matrix of the interchange process and c is the second smallest eigenvalue of $\mathbf{L}(P)$ such that $0 < c < 1$.*

Proof. The result follows by extending the result presented in Caputo et al. (2010) for continuous-time Markov chains to discrete-time Markov chains. In Caputo et al. (2010), the authors proved that the interchange process and the one-particle random walk have the same spectral gap in the case of reversible continuous-time Markov chains (see Theorem 1.1 therein). Their results can be extended to discrete time because, as stated in Section 3.4 of Aldous & Fill (2002), for a discrete-time chain and its continuization (*i.e.*, the transition rates are taken as $q_{ij} = p_{ij}$ for $j \neq i$), assuming the chain is reversible with uniform stationary distribution, the eigenvalues are related by $\lambda_m^{(c)} = 1 - \lambda_m^{(d)}$, where superscripts (c) and (d) indicate continuous and discrete time, respectively.

As noted in Aldous & Fill (2002), this relation holds for the basic discrete- and continuous-time random walks on a graph. Thus, we deduce that the spectral gaps of the discrete-time interchange process and random walk are equal: $\gamma^{IP} = \gamma^{RW}$. Recall that the one-particle random walk is the Markov chain with state space V in which a single particle jumps from node i to node $j \neq i$ with probability p_{ij} . Its discrete-time transition matrix is given by $\mathbf{I}_n - \mathbf{L}(P)$. The spectral gap of this random walk is $\gamma^{RW} = 1 - (1 - c)$, which concludes the proof. \square

E.2. Concentration Bounds for GoRank Estimates

Let $k \in [n]$. We now derive concentration bounds for the GoRank estimate $R_k(t)$ at node k with rank r_k at iteration t . Notice that the GoRank estimate can be written as the following empirical mean:

$$R'_k(t) = \frac{1}{t} \sum_{s=1}^t f_k(\eta_s),$$

where the samples are generated by the interchange process $\{\eta_s\}_{s \geq 1}$ and we define $f_k(\eta) = \mathbb{I}\{a_k > a_{\eta(k)}\}$, with $\eta(k)$ denoting the k -th component of the permutation $\eta \in S_n$. Its expectation under the stationary distribution is

$$\mathbb{E}_\pi[f_k(\eta)] = \frac{1}{n!} \sum_{\eta \in S_n} \mathbb{I}\{a_k > a_{\eta(k)}\} = \frac{1}{n} \sum_{l=1}^n \mathbb{I}\{a_k > a_l\} = r'_k.$$

We now present the following Hoeffding-type bound adapted from A. León & Perron (2004). According to the authors, the bound is optimal in the sense that the exponential rate is achieved asymptotically for a class of Markov chains.

Theorem E.3 (Hoeffding Type Bound). *The GoRank estimate satisfies the following Hoeffding-type bound: for all $u > 0$,*

$$\mathbb{P}_\pi(|R_k(t) - r_k| \geq u) \leq 2 \exp\left(-\frac{2}{2-c} \cdot ctu^2n^{-2}\right).$$

Proof. As stated in Lemma E.1, the Markov chain of the interchange process $\{\eta_t\}_{t \geq 1}$ is finite, ergodic and reversible with uniform stationary distribution π . Thus, we can apply the Hoeffding-type bound given in A. León & Perron (2004) (see Theorem 1 therein). Moreover, from Lemma E.2, the spectral gap of the chain is $1 - \lambda = c$ with $\lambda > 0$. We also note that $f_k \in [0, 1]$. Applying Theorem 1 of A. León & Perron (2004) with $\mu = r'_k$, we obtain for all $\varepsilon > 0$,

$$\mathbb{P}_\pi(R'_k(t) - r'_k > \varepsilon) \leq \exp\left(-\frac{1-\lambda}{1+\lambda} \cdot 2t\varepsilon^2\right).$$

Substituting $c = 1 - \lambda$, and using $u = n\varepsilon$, we obtain

$$\mathbb{P}_\pi(R_k(t) - r_k > u) \leq \exp\left(-\frac{c}{2-c} \cdot 2tu^2n^{-2}\right).$$

The same bound holds for $\mathbb{P}_\pi(R_k(t) - r_k < -u)$, which yields the two-sided inequality and completes the proof. \square

Similarly we derive a Bernstein-type adapted from Paulin (2015).

Theorem E.4 (Bernstein's Bound). *The GoRank estimate satisfies the following Bernstein-type bound: for all $u > 0$,*

$$\mathbb{P}_\pi(|R_k(t) - r_k| \geq u) \leq 2 \exp\left(-\frac{1}{4V_f + 10un^{-1}} \cdot ctu^2n^{-2}\right),$$

where $V_f = r'_k(1 - r'_k)$.

Proof. As stated in Lemma E.1, the Markov chain of the interchange process $\{\eta_t\}_{t \geq 1}$ is ergodic and reversible with uniform stationary distribution π . Thus, we can apply the Bernstein-type bound given in Paulin (2015) (see Theorem 3.3 therein). Moreover, from Lemma E.2, the spectral gap of the chain is $\gamma = c$ with $\lambda > 0$. Applying Theorem 3.3 of Paulin (2015) with $C = 1$, $V_f = r'_k(1 - r'_k)$, we obtain

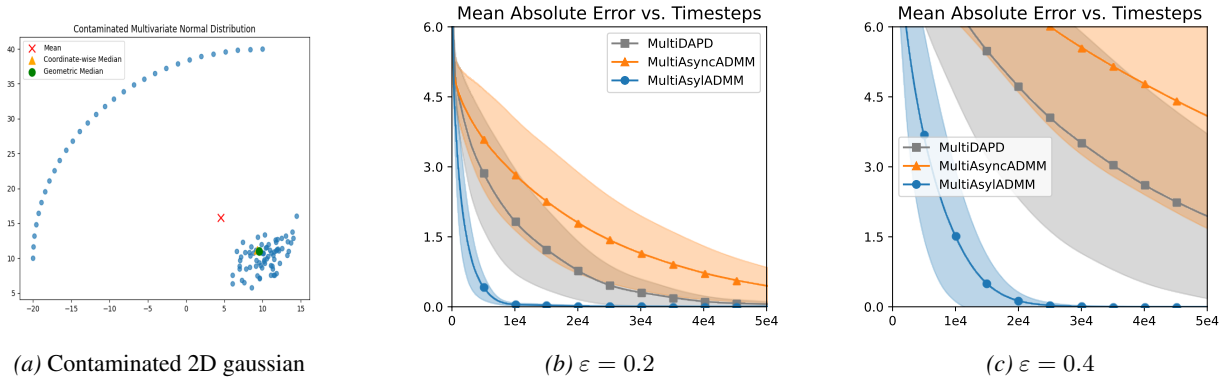
$$\mathbb{P}_\pi(|R'_k(t) - r'_k| \geq \varepsilon) \leq 2 \exp\left(-\frac{1}{4V_f + 10\varepsilon} \cdot \gamma t \varepsilon^2\right).$$

Substituting $\gamma = c$, and using $u = n\varepsilon$ completes the proof. \square

F. Additional Experiments for Section 4.3

F.1. Impact of contamination level ε using Setup of Fig 2a

We evaluate geometric median estimation using a two-dimensional contaminated Gaussian distribution. The clean data is drawn from a bivariate normal distribution with mean $\mu = (10, 10)^\top$ and covariance matrix $\Sigma = [[5, 3], [3, 5]]$. To simulate adversarial contamination, we introduce outliers uniformly distributed on a circular arc centered at the mean with radius 30. The contamination rate is $\varepsilon = 0.3$, and the total sample size is $n = 101$. We observe that contamination level has an impact on the convergence rate.



(a) Contaminated 2D gaussian

(b) $\varepsilon = 0.2$

(c) $\varepsilon = 0.4$

Figure 6. We compare existing optimization methods on geometric median estimation under various contamination levels.

F.2. Impact of trimming level α and contamination level ε using Setup of Fig 2b

We compare rank-based versus quantile-based trimming using the same setup as Plot (b) in Figure 1. Specifically, we consider a contaminated Gaussian distribution with contamination level $\varepsilon = 0.2$ (*i.e.*, 20% of the data is contaminated) and a trimming level of $\alpha = 0.3$. We evaluate performance using the mean absolute error of the estimated weights, which indicate whether each observation should be included. For quantile-based trimming, the weight at node k is defined as $W_k(t) = \mathbb{I}\{X_k \in [q_k^\alpha(t), q_k^{1-\alpha}(t)]\}$, where $q_k^\alpha(t)$ and $q_k^{1-\alpha}(t)$ are the quantile estimates obtained via AsylADMM. For rank-based trimming, the weight is given by $W_k(t) = \mathbb{I}\{R_k(t) \in I_{n,\alpha}\}$, where $R_k(t)$ is the rank estimate computed via Asynchronous GoRank and $I_{n,\alpha}$ is defined in Section 4.2. The results demonstrate that quantile-based trimming significantly outperforms rank-based trimming, particularly in later iterations where it achieves perfect accuracy. We investigate the impact of the trimming level α and contamination level ε across various graph topologies. Quantile-based trimming consistently outperforms rank-based trimming on sparse graphs. However, on complete graphs, rank-based trimming performs well, whereas quantile-based trimming converges slower, particularly when both α and ε are high.

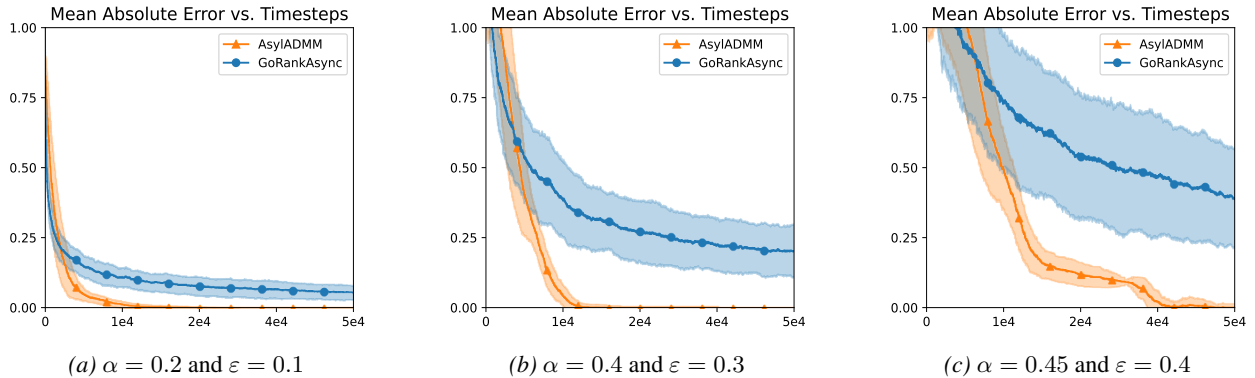


Figure 7. Comparison of quantile-based (AsylADMM) versus rank-based trimming (Asynchronous GoRank). The setup follows Plot (a) in Section 3 with varying trimming levels α and contamination levels ε . Plots (a)–(c) use a geometric graph.

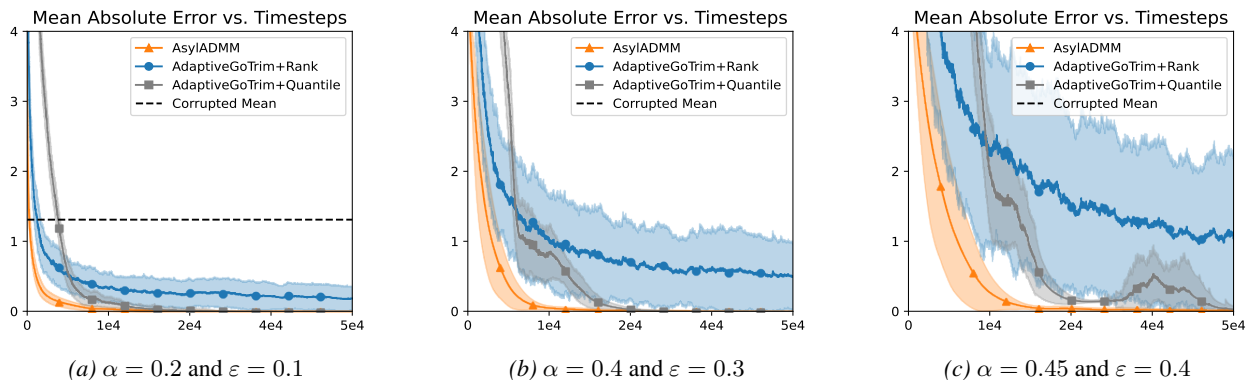


Figure 8. Comparison of median (AsylADMM), quantile-based trimmed mean (GoTrim+AsylADMM) and rank-based trimmed-mean (GoTrim+AsynGoRank). The setup follows Fig 2b. with varying trimming levels α and contamination levels ε . Plots (a)–(c) use a geometric graph.

F.3. Impact of trimming level α and contamination level ε using Setup of Fig 2c

Figure 9 corresponds to the same experimental setting as Fig. 2c, examining performance across varying trimming levels, contamination levels, and graph topologies. Figure 10 presents the mean absolute error of the GoDepth algorithm, specifically, the error in L_2 depth estimation as well as the error in estimating the α -quantile of the depths.

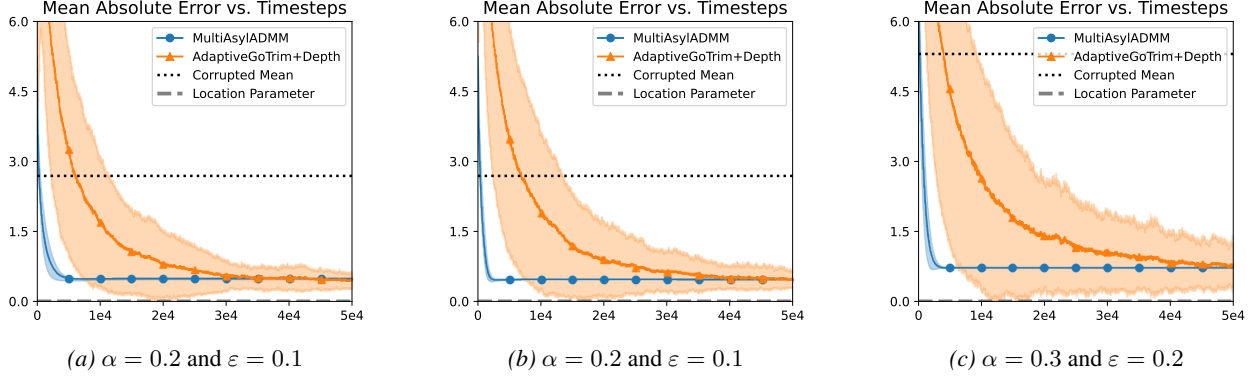


Figure 9. Comparison of geometric median (AsylADMM) with depth-based trimming. The setup follows Plot (c) in Section 4 with varying trimming levels α and contamination levels ε . Plot (a) uses a geometric graph and (b)-(c) use a Watts-Strogatz graph.

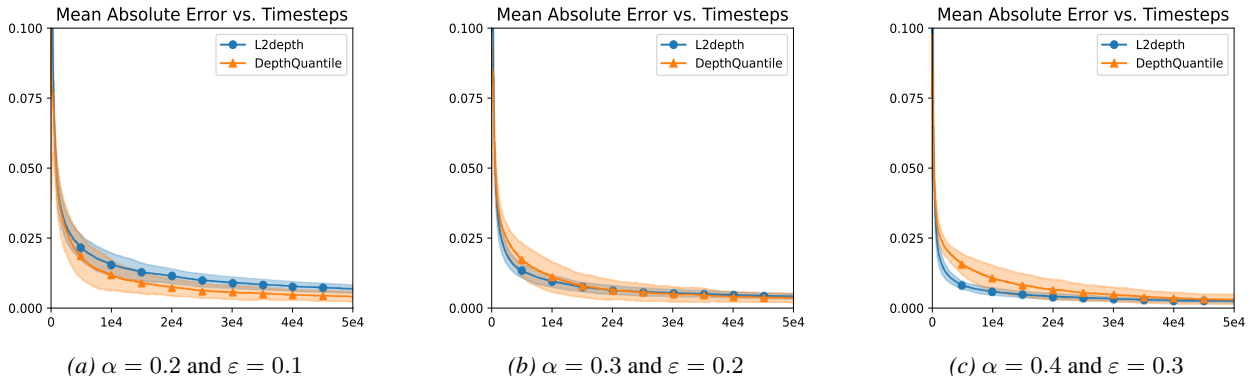


Figure 10. Empirical performance of depth estimation with corresponding quantile estimation on geometric graph.

G. Convergence Analysis of Asyl-ADMM

1. Supermartingale convergence We use the symbol \mathcal{F}_t to denote the filtration up to t . We have $\mathcal{F}_t \subset \mathcal{F}_{t+1}$ for all $t \geq 1$. We have the following result on supermartingale convergence.

Theorem(Robbins-Siegmund): Let $\{e_t\}, \{u_t\}, \{\delta_t\}$ be non-negative \mathcal{F}_t -adapted sequences. If:

$$\mathbb{E}[e_{t+1} \mid \mathcal{F}_t] \leq e_t - \alpha_t + \delta_t$$

with $\sum_t \delta_t < \infty$, and $\alpha_t \geq 0$, then: 1. e_t converges a.s. to some random variable $e_\infty \geq 0$ 2. $\sum_t \alpha_t < \infty$ a.s.

2. Proof Intuition and Technical Obstacles We begin by introducing the centered variables $\tilde{\mu}_k^{t+1}(e) = \mu_k^{t+1}(e) - \mu_k^*$ and $\tilde{x}_k^{t+1}(e) = x_k^{t+1}(e) - x^*$, where $\mu_k^{t+1}(e)$ and $x_k^{t+1}(e)$ denote the updates to μ_k^t and x_k^t , respectively, when edge e is activated. We also define the residual $R_{e,k}^{t+1}(e) = z_e^{t+1} - x_k^{t+1}(e)$.

Following the approach used in the synchronous setting, we apply bounds I and II to $f(\hat{x})$, where $\hat{x} = (\hat{x}_1, \dots, \hat{x}_n)$ with $\hat{x}_k = \frac{1}{d_k} \sum_{e \in N_k} x_k(e)$. By convexity of f , we have $\tilde{f}_k(\hat{x}_k) \leq \frac{1}{d_k} \sum_{e \in N_k} \tilde{f}_k(x_k^{t+1}(e))$. Applying the optimality condition (subgradient inequality) for each $\tilde{f}_k(x_k^{t+1}(e))$ and summing the resulting inequalities yields

$$0 \leq \sum_k \sum_{e \in N_k} \left(\rho R_{e,k}^{t+1}(e) + \frac{\tilde{\mu}_k^{t+1}(e)}{d_k} \right)^\top \tilde{x}_k^{t+1}(e).$$

A key property exploited in the synchronous analysis is the antisymmetry of dual variables, which ensures $\sum_k \sum_{e \in N_k} y_{e,k}^\top z_e = 0$. While antisymmetry still holds for the true dual variables, using $\hat{\mu}_k(e)$ as a surrogate breaks this property: in general, $\sum_k \sum_{e \in N_k} \hat{\mu}_k(e)^\top z_e \neq 0$. Consequently, we cannot directly transform the term $(\hat{\mu}_k^{t+1}(e))^\top \tilde{x}_k^{t+1}(e)$ into an expression involving only the residual. Had this been possible, we would obtain

$$\sum_k \sum_{e \in N_k} \left(\frac{\tilde{\mu}_k^{t+1}(e)}{d_k} - \rho \tilde{x}_k^{t+1}(e) \right)^\top R_{e,k}^{t+1} \leq 0.$$

The discrepancy arises from the additional term $A(t) = \left| \sum_k \sum_{e \in N_k} \frac{1}{d_k} \mu_k(e)^\top z_e \right|$. Intuitively, this term should be small since $\sum_k \sum_{e \in N_k} \frac{1}{d_k} \mu_k(e) = 0$, or at least bounded by a quantity depending on the residual, such as $\sum_{k,e} \|z_e - x_k\|^2$. Empirically, we observe that $A(t) \rightarrow 0$ as $t \rightarrow \infty$.

We now define the Lyapunov function. Let $V_k^{t+1}(e) = \left\| \frac{\tilde{\mu}_k^{t+1}(e)}{d_k} - \rho \tilde{x}_k^{t+1}(e) \right\|^2$ and $V^{t+1} = \sum_k \left\| \frac{\tilde{\mu}_k^{t+1}}{d_k} - \rho \tilde{x}_k^{t+1} \right\|^2$. Taking conditional expectations, we obtain

$$\mathbb{E}[V^{t+1} \mid \mathcal{F}_t] = \sum_k \left(\sum_{e \in N_k} p_e V_k^{t+1}(e) + (1 - \alpha_k) V_k^t \right),$$

since it's the sum of $\sum_e (\sum_{k \in e} V_k^{t+1}(e) + \sum_{k \notin e} V_k^t)$.

$$\mathbb{E}[\Delta V^{t+1} \mid \mathcal{F}_t] = \sum_k \sum_{e \in N_k} p_e (V_k^{t+1}(e) - V_k^t).$$

Assuming the previous inequality holds (which, as noted, it does not due to the extra term $A(t)$), we would have

$$\mathbb{E}[\Delta V^{t+1} \mid \mathcal{F}_t] \leq -\frac{\rho^2}{2} \sum_k \sum_{e \in N_k} p_e \|R_{e,k}^{t+1}\|^2.$$

Defining $\bar{R}^{t+1} = \sum_k \sum_{e \in N_k} p_e \|R_{e,k}^{t+1}\|^2$, this simplifies to

$$\mathbb{E}[\Delta V^{t+1} \mid \mathcal{F}_t] \leq -\frac{\rho^2}{2} \bar{R}^{t+1}.$$

Setting $\alpha_t = \bar{R}^{t+1}$ and $e_t = V^t$, standard supermartingale arguments would imply that V^t is almost surely bounded and $\sum_{t=0}^\infty \bar{R}^{t+1} < \infty$. From this, objective convergence would also follow.

H. Comparison of Synchronous versus Asynchronous setting

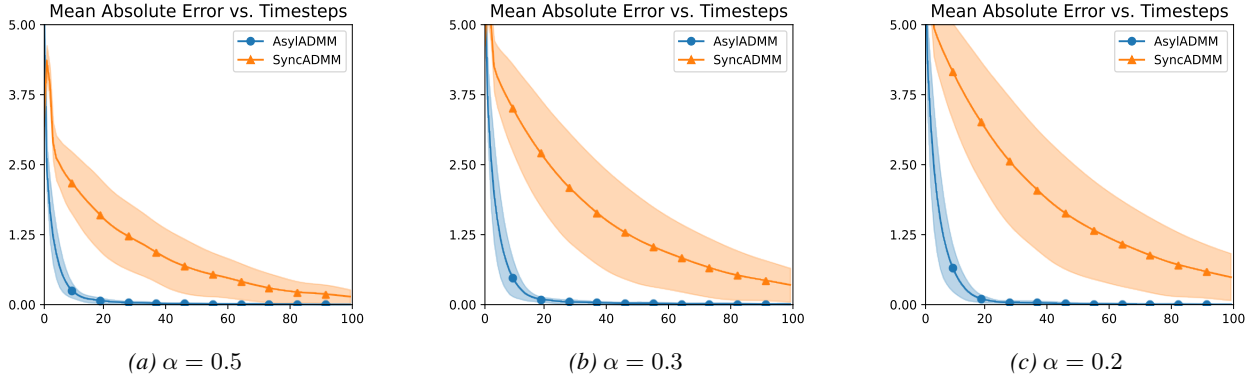


Figure 11. Comparison of AsyIADMM versus its synchronous variant on median/quantile estimation using a geometric graph with 101 nodes. One iteration corresponds to one full graph use ($|E|$ asynchronous updates).

I. Robust Regression via Trimming

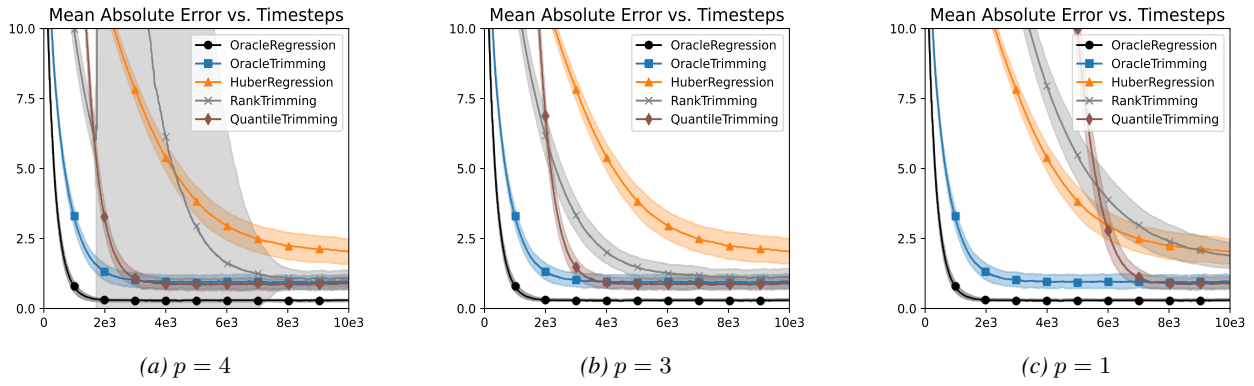


Figure 12. Comparison of rank-based trimming and quantile-based trimming on robust regression problem with varying parameter p .

We apply rank-based and quantile-based trimming to robust regression; see Appendix D. We generate a synthetic dataset of 101 data points (x_k, y_k) for linear regression and contaminate 10% of the dataset with arbitrary Gaussian noise. The contamination is designed such that, without robustness mechanisms, the regression prediction is completely corrupted. We compare our methods against two baselines: OracleRegression, which is trained only on the non-contaminated portion of the dataset, and OracleTrimming, which is trained with the m nodes having the highest scores excluded. We set the trimming level to $\alpha = 0.2$. Specifically, we remove gradients from nodes whose data points yield scores $d_k = -|x_k| \cdot |y_k|$ in the bottom $m = \lfloor \alpha n \rfloor$ of all scores. This can be implemented either by ranking the d_k values and identifying points with ranks $r_k \leq m$, or by computing the boundary quantile q^α and selecting data points satisfying $d_k \leq q^\alpha$. Since rank and quantile estimation require time to stabilize, we augment the rules in two different ways. For rank-based trimming, we add an uncertainty term $\delta_k(t) = 4np^{-1} / \sqrt{c_k(t)}$, where $c_k(t)$ denotes the number of updates performed by node k . This term decreases over iterations, yielding the modified inclusion rule $R_k(t) > m + \delta_k(t)$. For quantile-based trimming, we impose a burn-in period by waiting until $c_k(t) > 4np^{-1}$ iterations before applying the exclusion rule $d_k > q^\alpha(t)$; during this period, no gradients are included. We evaluated both methods with varying values of the parameter p . For rank-based trimming, we found that $p = 4$ leads to divergence, while $p = 1$ results in overly slow convergence. With $p = 3$, both methods converge reliably, and our approach achieves performance competitive with classical Huber regression.

J. Additional Experiments on the Edge-Based Algorithm of Wei & Ozdaglar (2013)

In Wei & Ozdaglar (2013), the ADMM problem was reformulated using an edge-based approach; however, this formulation appears not to converge (see experiments below). The key idea is as follows. For each edge $e = (i, j)$, the constraint $x_i = x_j$ is decomposed using auxiliary variables: $x_i = z_{ei}$, $-x_j = z_{ej}$, and $z_{ei} + z_{ej} = 0$. This can be written compactly as $A_{ei}x_i = z_{ei}$, where A_{ei} denotes the entry in the e -th row and i -th column of the incidence matrix A , which is either 1 or -1. The corresponding algorithm is given below; see Section D in Wei & Ozdaglar (2013):

1. Initialization: choose some arbitrary x_i^0 in X and z^0 in Z , which are not necessarily all equal. Initialize $p_{ei}^0 = 0$ for all edges e and end points i .

2. At time step k , the local clock associated with edge $e = (i, j)$ ticks,

a) Agents i and j update their estimates x_i^k and x_j^k simultaneously as

$$x_q^{k+1} = \underset{x_q \in X}{\operatorname{argmin}} f_q(x_q) - (p_{eq}^k)' A_{eq} x_q + \frac{\beta}{2} \|A_{eq} x_q - z_{eq}^k\|^2$$

for $q = i, j$. The updated value of x_i^{k+1} and x_j^{k+1} are exchanged over the edge e .

b) Agents i and j exchange their current dual variables p_{ei}^k and p_{ej}^k over the edge e . For $q = i, j$, agents i and j use the obtained values to compute the variable v^{k+1} as Eq. (20), i.e.,

$$v^{k+1} = \frac{1}{2} (-p_{ei}^k - p_{ej}^k) + \frac{\beta}{2} (A_{ei} x_i^{k+1} + A_{ej} x_j^{k+1}).$$

and update their estimates z_{ei}^k and z_{ej}^k according to Eq. (19), i.e.,

$$z_{eq}^{k+1} = \frac{1}{\beta} (-p_{eq}^k - v^{k+1}) + A_{eq} x_q^{k+1}.$$

c) Agents i and j update the dual variables p_{ei}^{k+1} and p_{ej}^{k+1} as

$$p_{eq}^{k+1} = -v^{k+1} \quad \text{for } q = i, j.$$

We tested the method with various step sizes and using the settings from Fig. 1a. We compared it with AsyIADMM using $\rho = 1.0$. The results are shown Figure 13.

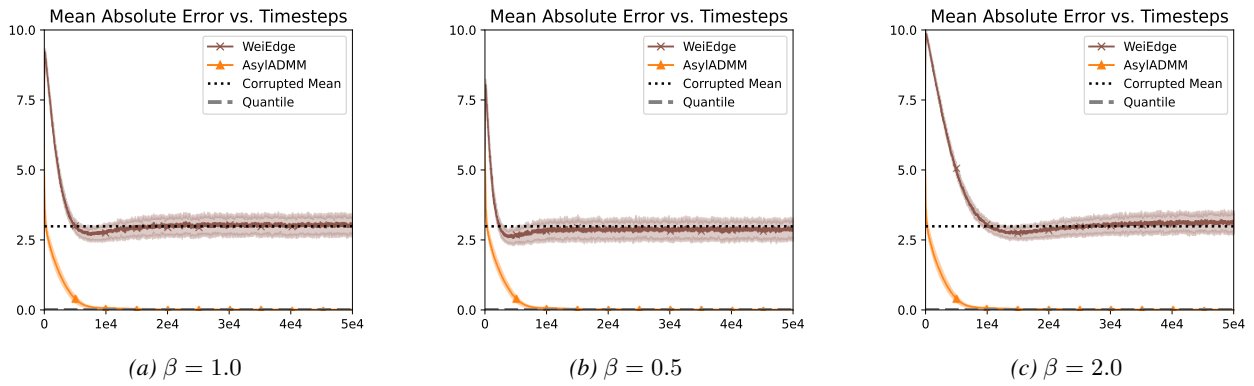


Figure 13. The edge-based formulation from Wei & Ozdaglar (2013) fails to converge on the median estimation problem.